persons [23], habitual alcohol drinkers [24], infants and pregnant/parturient women [22] have the tendency to develop Zn deficiency. In addition, maternal Zn deficiency during pregnancy induces pregnancy complications, delayed delivery, and low-body-weight birth [25]. Zn deficiency is responsible for 4.4% of deaths of children aged 6–59 months in developing countries [26].

Metallothionein (MT), a low-molecular weight protein, has been shown to be involved in the transport, metabolism and homeostasis of heavy metal ions, such as Zn and copper, in tissues and cells. One-third of their amino acid residues of this protein are cysteine residues without a disulfide bond. This characteristic enables MTs to play a role in the transport and inactivation/detoxification of metals [27,28]. Aside from the metabolism and homeostasis of heavy metals, MT has been known to protect cells from oxidative stress and inflammation elicited by various environmental stimuli including heavy metals. Among the four MT isoforms known so far, MT1 and MT2 exist in nearly all types of cells in the body. It has been established that the expression of *MT1/2* genes is induced by metal ions, such as Cd, Zn, Cu and Hg [27]. For the up-regulation of *MT1/2* transcription upon exposure to these metal ions, metal responsive elements (MREs) located in the promoter region are essential. A limited line of experimental evidence showed that metal transcription factor 1 (MTF1) [29] will bind to the MRE motif upon exposure to at least Zn ions, and the Zn-ion-bound MTF1 forms a complex with p300 and Sp1, and then this complex is recruited to MREs of the *MT1* promoter region [30].

The effects of prenatal zinc deficiency on MT regulation have been studied. Pregnant mice were fed either a control diet (100 μg Zn/g) or a low-Zn diet (5.0 μg Zn/g) from gestation day 7 to delivery, and both groups of dams were given the control diet after delivery. Although the Zn and MT levels in pups born to these two groups of dams were similar at postnatal day 3, serum IgM concentrations were significantly lower in adulthood in the mouse offspring born to dams given the low-Zn diet than in the offspring born to control dams. Moreover, when the mouse offspring was given Zn injections to stimulate MT synthesis, the mice deprived of Zn while *in utero* had markedly higher MT levels in the liver than control mice later in adulthood [31].

Collectively, prenatal Zn deficiency has been shown to induce disease states, which is presumably due to epigenetic alterations. However, nearly no studies to elucidate the molecular basis of disease states induced by prenatal Zn deficiency are available. Thus, we have hypothesized that fetal epigenetic alterations can be induced by Zn deficiency *in utero* and alter the physiological conditions that will lead to the onset of disease conditions later in adulthood. In this study, we developed an experimental animal model of prenatal Zn deficiency and studied whether Zn deficiency *in utero* exerts fetal epigenetic alterations in *MT1/2* genes.

2. Materials and methods

2.1. Reagents

The following reagents were purchased from the manufacturers described in parentheses: RNase A, mouse monoclonal anti-β-actin IgG1 and CellLyticNuCLEARExtraction kit (Sigma-Aldrich, St Louis, MO, USA); RNeasy Mini kit, QIAquick PCR Purification kit, QIAquick Gel Extraction kit and QIAprep Spin Miniprep kit (Qiagen K.K., Tokyo, Japan); Lipofectamine 2000 (Invitrogen, Carlsbad, CA, USA); Wizard DNA Clean-Up system, pGEM-T Easy Vector, pGL4.0 Luciferase Reporter Vector, phRL-TK Vector and Dual-Luciferase Reporter Assay System (Promega, Madison, WI, USA); proteinA agarose/salmon sperm DNA, rabbit polyclonal anti-acetylated histone H3 IgG, rabbit polyclonal anti-acetylated histone H4 IgG, rabbit polyclonal anti-acetylated histone H3 lysine14 IgG and Immobilon-P transfer membrane (MilliPore, Billerica, MA, USA); proteinase K, Blocking One and Chemi-Lumi One (Nacalai Tesque, Kyoto, Japan, USA). *Bam* HI, *Aci* I, *Kpn* I, *Xho* I and *Dpn* I were purchased from New England Biolabs Japan (Tokyo, Japan); rabbit polyclonal anti-MTF1 IgG and goat polyclonal anti-lamin B (Santa Cruz Biotechnology, Santa Cruz, CA, USA); Big Dye Terminator v3.1 Cycle Sequencing kit (Applied Biosystems, Foster City, CA, USA); Immunopure goat anti-rabbit IgG, F(ab′)2, peroxidase conjugated, ImmunoPure goat anti-mouse IgG, F(ab′)2, peroxidase conjugated and Immuno Pure rabbit anti-goat IgG, F(ab′)2, peroxidase conjugated (Thermo Fisher Scientific, Rockford, IL, USA); rabbit polyclonal anti-acetylated histone H3 lysine9 IgG and rabbit polyclonal anti-trimethylated histone H3 lysine4 IgG (Cell Signaling Technology, Danvers, MA, USA). LightCycler480 SYBR Green I Master (Roche Diagnostics Japan, Tokyo, Japan); Minisart SRP 15 (Sartorius Stedim Biotech, Goettingen, Germany). IGEPAL-CA630 (Wako Pure Chemical, Osaka, Japan); PrimeScript RT reagent kit, SYBR Premix Ex Taq, TaKaRa Ex Taq, LA Taq and T4 polynucleotide kinase (TaKaRa BIO, Otsu, Japan). *Not* I, DH5α and KOD -Plus (Toyobo, Osaka, Japan); Ligation Convenience kit and ISOGEN (Nippon Gene, Tokyo, Japan); all other reagents of analytical grade (Sigma-Aldrich, Invitrogen and Wako Pure Chemical); all oligonucleotides (Hokkaido System Science, Sapporo, Japan).

2.2. Animals

C57BL/6J strain pregnant ($n=44$) and male mice ($n=18$) were purchased from CLEA Japan. The mice were housed in a room with temperature at 23±1°C and humidity at 50±10% on a 12/12-h light–dark cycle. We used three kinds of rodent chow. Laboratory rodent chow (50 μg Zn/g; Labo MR Stock, Nosan) was given to mice unless specifically described. Low-Zn diet (5.0 μg Zn/g) or control diet (35 μg Zn/g) (CLEA Japan) was used in Zn-deficiency experiments. According to the previous studies [32,33], zinc concentration in diet (35 μg Zn/g) was found to be high enough to be used for a control diet group. These chows and deionized water were provided *ad libitum*. For this study, male mice were used unless specifically described. The experiments protocols using mice were approved by the Animal Care and Use Committee of the Graduate School of Medicine, the University of Tokyo.

2.3. Experiments on Zn deficiency in utero

Pregnant mice were fed a Labo MR Stock rodent chow until gestation day 7, and the chow was replaced with a low-Zn diet or a control diet thereafter until delivery. On the day of birth, two to three male pups per dam were randomly adopted from fourteen dams to minimize possible litter effects and to make two groups: (1) *in utero* low-Zn (IU-LZ) mice and (2) *in utero* control (IU-CZ) mice. The pups were decapitated by scissors, and their livers were harvested. All the liver tissues except those used for chromatin immunoprecipitation (ChIP) assay were immediately frozen in liquid nitrogen, and kept at −80°C until analyses. Livers used for the ChIP assay were immediately minced by scissors and subjected to the subsequent processes as described in the ChIP assay section below. The number of pups for each dam was adjusted to be 6 to 7 pups by adoption from other dams on the day of birth. The dams were given Labo MR Stock rodent chow from the delivery to weaning. After weaning, male pups were given Labo MR Stock rodent chow thereafter.

When IU-CZ mice and IU-LZ mice became 5 weeks old, they were administered orally with a single dose of cadmium (Cd) (5.0 mg kg^{-1} b.w.). Mice were sacrificed by cervical dislocation, and livers were harvested 0, 1 and 6 h post Cd administration (Fig. 1A).

2.4. Experiment on Zn deficiency in adulthood

Male mice aged 10 weeks were fed a low-Zn(AD-LZ) diet or a control (AD-CZ) diet *ad libitum* for 12 days, and then sacrificed by cervical dislocation to harvest the liver. Other mice were fed Labo MR Stock rodent chow for another 30 days, and administered orally a single dose of Cd (5.0 mg kg^{-1} b.w.). Livers were collected 6 h after Cd administration (Fig. 1B).

2.5. Measurement of Zn and Cd concentrations

Livers (approx. 0.1 g) and blood (approx. 0.2 g) specimens were digested in 2 ml of concentrated nitric acid in glass test tubes. The temperatures were kept at 80°C for 1 h, with a gradual increase with 10°C for 1 h each to 130°C. When the acid-digested specimens were became transparent, they were diluted with 1% $HNO_3$and filtered with Minisart SRP 15 and determined for Zn and Cd concentrations by inductively coupled plasma mass spectrometer (Agilent 7500ce; Agilent Technologies).

2.6. RNA isolation and reverse transcription

Total RNA was isolated using RNeasy Mini Kit and then reverse-transcribed using PrimeScript RT reagent Kit, according to the manufacturer's instructions.

2.7. DNA isolation

DNA was isolated using ISOGEN, according to the manufacturer's instructions and purified by phenol/chloroform extraction method.

2.8. Quantitative polymerase chain reaction

Quantitative polymerase chain reaction (qPCR) analysis was performed using SYBR Premix Ex Taq and amplified by LightCycler under the following conditions: 95°C/10 s ×1 cycle; 95°C/5 s, 60°C/30 s, ×45 cycles or using LightCycler480 SYBR Green I Master and amplified by LightCycler480 under the following conditions: 95°C/5 min ×1 cycle; 95°C/15 s, 60°C/10 s, 72°C/30 s ×45 cycles. Primers used in the qPCR analysis

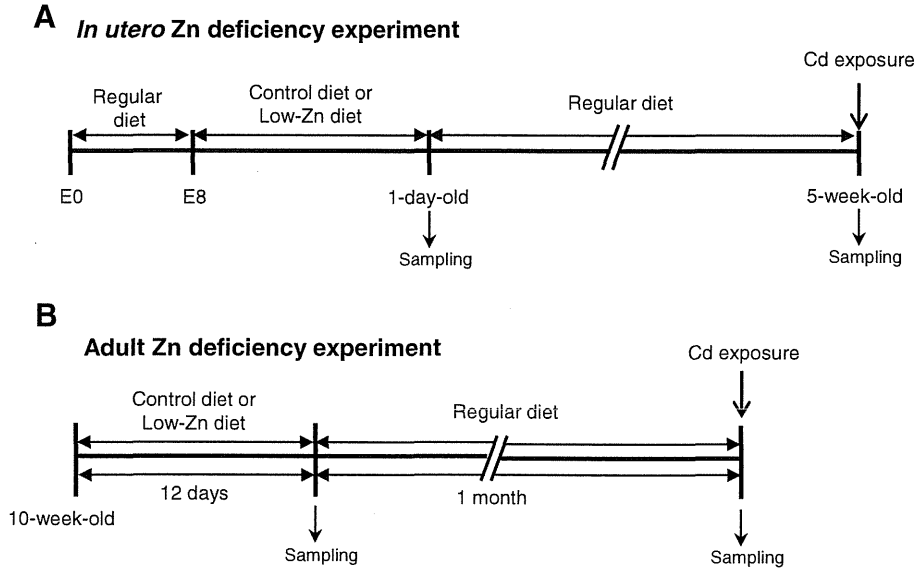

Fig. 1. Study design. (A) Pregnant mice were fed a regular diet until Gestation Day 7, and the chow was replaced with a low-Zn diet or control diet thereafter until delivery. On the day of birth, male pups were divided into two groups: (1) *in utero* low-Zn (IU-LZ) mice and (2) *in utero* control-Zn (IU-CZ) mice. Livers were harvested from a group of 1-day-old male pups. The dams were given Labo MR Stock rodent chow from the delivery to weaning. After weaning, male pups were given Labo MR Stock rodent chow thereafter. When IU-CZ mice and IU-LZ mice became 5 weeks old, they were administered orally a single dose of Cd (5.0 mg kg^{-1} b.w.) and sacrificed by cervical dislocation, and livers were collected 0, 1 and 6 h after Cd administration. (B) Male mice aged 10 weeks were fed a low-Zn diet (AD-LZ) or control diet (AD-CZ) ad libitum for 12 days and then sacrificed by cervical dislocation, and livers were collected. Other mice were fed a regular diet for another 30 days and administered orally a single dose of Cd (5.0 mg kg^{-1} b.w.). Livers were collected 6 h after Cd administration.

are described in Table S1. All primer sets were designed by using Primer3 [34]. All quantitative data were calculated by dividing the copy number of targets by the original RNA concentration, according to a previous study [35].

2.9. Bisulfite genomic sequencing

Mouse genomic DNA was digested with *Not* I and bisulfite conversion reaction was performed as previously described [36]. The bisulfite-treated DNA was cleaned up using Wizard DNA Clean-Up system and amplified by nested PCR method using Ex Taq under the following conditions for the first and second PCRs: 94°C/2 min ×1 cycle; 94°C/2 min, 50°C/2 min, 72°C/3 min, ×5 cycles; 94°C/2 min, 50°C/2 min, 72°C/30 s, ×5 cycles; 72°C/5 min ×25 cycles. Each primer set for the nested amplification is shown in Table S2. All primers were designed using Methyl Primer Express Software v1.0 (Applied Biosystems). The amplified DNA was purified using QIA quick PCR Purification kit and ligated into pGEM-T Easy Vector and transformed into DH5α. Colony PCR was performed to amplify target DNAs using Ex Taq and M13 primers. The PCR products were sequenced using Big Dye Terminator v3.1 Cycle Sequencing kit and analyzed using 3730 DNA Analyzer (Applied Biosystems).

2.10. Methylation frequency analysis

Purified DNA was digested with *Bam* HI. The digested DNA solution was divided into two portions. One portion was digested with the methylation-sensitive *Aci* I, whereas the other was kept as it was. These *Aci* I-digested and non-digested DNA was subjected to qPCR using SYBR Premix Ex Taq and amplified by LightCycler under the following conditions: 95°C/10 s ×1 cycle; 95°C/5 s, 60°C/15 s, 72°C/20 s, ×40 cycles. Ch-R1 primer sets described in Table S3. The DNA methylation frequency was represented as copy numbers of *Aci* I-digested DNA/copy numbers of non-digested DNA.

2.11. Chromatin Immunoprecipitation assay

The ChIP assay was performed by the essentially same method as previously described [37], with some modifications: the minced mouse liver was cross-linked with 1% formaldehyde for 10 min at room temperature, followed by addition of glycine to be a final concentration of 125 mM and by incubation for 5 min. The cross-linked liver specimen was homogenized using a Dounce homogenizer (catalog# 432–1273, Wheaton) and washed with phosphate-buffered saline three times. The pellet was dissolved in lysis buffer (5.0 mM Tris–HCl, pH 8.1, containing 1.0% sodium docecyl sulfate [SDS], 10 mM EDTA). It was subjected to sonication by Bioruptor UCD-250HSA (Cosmo Bio) to make an average chromatin fragment size to be 200 to 1000 bp. ProteinA agarose and salmon sperm DNA were added to the fragmented DNA solution, and it was incubated for 1 h at 4°C to eliminate nonspecific substances. An aliquot of the sample was diluted by adding dilution buffer (16.6 mM Tris–HCl, pH 8.1, containing 0.01% SDS, 1.1% Triton X-100, 1.2 mM EDTA, and 167 mM NaCl) and incubated with an antibody at 4°C overnight. The sample was immunoprecipitated with ProteinA agarose and salmon sperm DNA and washed consecutively with the following four kinds of buffers: low-salt immune complex buffer (20 mM Tris–HCl, pH 8.1, containing 0.1% SDS, 1.0% Triton X-100, 2.0 mM EDTA, and 0.15 M NaCl), high-salt immune complex buffer (20 mM Tris–HCl, pH 8.1, containing 0.1% SDS, 1.0% Triton X-100, 2.0 mM EDTA, and 0.5 M NaCl), LiCl immune complex buffer (10 mM Tris–HCl, pH 8.1, containing 1.0% IGEPAL-CA630, 1.0 mM EDTA, 0.25 M LiCl, 1.0% deoxycholic acid), and TE buffer. The immunoprecipitated DNA was eluted with buffer (0.1 M $NaHCO_3$, pH 8.5, containing 1.0% SDS and 10 mM DTT). Cross-link was removed by an addition of 5.0 M NaCl with incubation at 65°C overnight. The resultant DNA was treated with RNase A for 30 min and proteinase K for 1 h, and the DNA was purified by using QIA quick PCR Purification kit. Quantitative real time PCR was carried out with the DNA using SYBR Premix Ex Taq and amplified by LightCycler under the following conditions: 95°C/10 s ×1 cycle; 95°C/5 s, 60°C/15 s, 72°C/20 s, ×60 cycles or using LightCycler480 SYBR Green I Master and amplified by LightCycler480 under the following conditions: 95°C/5 min ×1 cycle; 95°C/15 s, 60°C/10 s, 72°C/30 s ×65 cycles. Primers used in this assay are described in Table S3.

2.12. Western blotting

Nuclear and cytosolic proteins were extaracted from mouse liver using CellLyticNuCLEARExtraction kit according to the manufacturer's instructions. The protein specimens (25 μg protein/lane) were separated on a 10% SDS-polyacrylamide gel and blotted on an Immobilon-P transfer membrane. The blotted membrane was blocked with Blocking One at room temperature for 1 h. Primary antibody was applied at 4°C overnight, with a dilution factor as described in parentheses: anti-MTF IgG (1:10,000), β-actin IgG1 (1:4,000) and anti-laminB IgG (1:1,000). The 5,000-fold diluted the secondary antibody was applied at room temperature for 1 h. The antigen-antibody complexes were visualized by using Chemi-Lumi One. For quantitative analysis, the chemiluminescence intensity of respective bands was quantified using CS analyzer ver.2.02b (ATTO).

2.13. Plasmid constructs

The DNA fragment containing *Kpn* I and *Xho* I restriction sites of −2,166 to −17 in the *MT2* promoter was amplified from mouse hepatic DNA by PCR method using LA Taq under the following conditions: 95°C/1 min ×1 cycle; 95°C/30 s, 60°C/1 min, 72°C/2 min, ×30 cycles; 72°C/10 min ×1 cycle. Primers used for the qPCR are described in Table S4. This fragment was inserted into pGEM-T Easy Vector using Ligation Convenience kit. This plasmid was transformed to DH5αand cloned. The cloned plasmid was digested by *Kpn* I and *Xho* I. The inserted fragment was separated by electrophoresis in agarose gel and purified by QIAquickGel extraction kit. This purified fragment was inserted into pGL4.0 Luciferase Reporter Vector digested by *Kpn* I and *Xho* I. This construct was named as *pGL4MT2 -2166*. The *MT2* MRE-deletion constructs

(Fig. 4B) were made from *pGL4MT2 -2166* as a template by inverse PCR method as follows. The MRE-deletion fragments were amplified from *pGL4MT2-2166* construct by PCR method using KOD-Plus under the following conditions: 94°C/2 min ×1 cycle; 98°C/10 s, 68°C/2 min, ×10 cycles. Primers used are described in Table S4. The remaining pGL4MT2 construct was digested by *Dpn* I. The 5′-prime of MRE-deletion fragments was phosphorylated by T4 polynucleotide kinase. These fragments were self-ligated by Ligation Convenience kit and transformed to DH5α. The cloned MRE-deletion constructs were purified by QIAprep Spin Miniprep kit.

2.14. Transfection and luciferase reporter assay

Hepa1c1c7 cells purchased from American Type Culture Collection were maintained in DMEM, supplemented with 10% FBS, 100 U/ml penicillin, 0.01% streptomycin, 0.01% sodium pyruvate, 0.03% L-glutamine, and 55 μM 2-mercaptethanol at 37°C under 5.0% CO_2 condition. In the first experiment, to examine induction of *MT2* mRNA by Cd exposure, cells were seeded at a density of 4.4×10^5 cells per well in a six-well multiplate. After 24 h, cells were exposed to 5.0 μM Cd for a specified time and harvested for qPCR analysis. In the second experiment, to study transcription activity of *MT2*, cells were seeded and incubated at a density of 4.4×10^5 cells per well in a 48-well multiplate for 24 h, followed by co-transfection with phRL-TK Vector and each MT2 reporter construct using Lipofetamine2000 for another 24 h. Then, the cells were exposed to 5.0 or 10.0 μM Cd for 24 h, and reporter assays were conducted using the Dual-Luciferase Reporter Assay System, following the manufacturer's instructions.

2.15. Statistical analysis

All results are expressed as mean±standard errors. Statistical analysis was performed using IBM SPSS Statistics ver. 19.0 (IBM). A two-way analysis of variance (ANOVA), followed by Bonferroni's post hoc test was performed to compare means of mRNA expression, histone modification, and protein expression among IU-LZ and IU-CZ or AD-LZ and AD-CZ groups of 5-week-old mice as well as reporter gene assay data. Student's *t* test was used for other analyses to compare between IU-LZ and IU-CZ groups or AD-LZ and AD-CZ groups. A *P*-value of less than .05 was considered to be statistically significant.

3. Results

3.1. Zn and Cd concentrations in liver

Pregnant mice fed the low-Zn diet had a significantly lower blood Zn concentration than those fed the control diet (3.98±0.04 μg/g, $n=3$ vs. 4.92±0.10 μg/g, $n=6$). As for the mouse progeny, no significant difference in body weight was observed between IU-LZ and IU-CZ mice on postnatal days 1, 27, and 35 (data not shown). The hepatic Zn concentration was significantly lower in 1-day-old IU-LZ mice than in IU-CZ mice (20.4±1.8 μg/g tissue, $n=13$ vs. 37.3±2.9 μg/g tissue, $n=18$), but they became similar by postnatal week 5 (Table 1). No significant changes in hepatic Zn and Cd concentrations were observed between IU-LZ and IU-CZ mice 6 h after Cd administration (Table 1).

3.2. Induction of MT1 and MT2 mRNAs upon Cd exposure in the liver of mice fed a Zn deficient-diet

The abundances of *MT1* and *MT2* mRNAs in the liver were examined in 5-week-old mice with and without Cd exposure. The abundances of *MT1* mRNAs in IU-LZ and IU-CZ mice at 6 h after Cd administration were significantly higher than those in the corresponding groups of mice at 0 h (Fig. 2A). Similar results to *MT1* mRNA were observed for *MT2* mRNA although no statistically significant observations were obtained for the abundance of *MT2* mRNA in IU-CZ before and after Cd administration (Fig. 2B). Without Cd exposure, the abundances of *MT1* and *MT2* mRNAs of IU-LZ mice and those of IU-CZ mice were not different from each other (Fig. 2A, B). Six hours after Cd administration, the abundances of *MT1* mRNA was similar between IU-LZ and IU-CZ mice (Fig. 2A), whereas the abundances of *MT2* mRNA was higher in IU-LZ mice than in IU-CZ mice (Fig. 2B). Although the elevated expression of *MT* genes has been shown to be mediated by MTF1 upon Zn administration [30], no significant alterations in *MTF1* mRNA abundance were found between IU-LZ and IU-CZ mice after Cd administration (Fig. 2C).

Table 1
Zn and Cd concentrations in the liver of 5-week-old mice born to dams given a low-Zn diet or a control diet and those before or after Cd administration

Experimental group	Zn (μg/g tissue)		Cd (μg/g tissue)	
	Unexposed	Cd-exposed	Unexposed	Cd-exposed
IU-CZ	32.2±0.5 (5)	42.8±1.2 (6)	n. d. (5)	0.71±0.13 (6)
IU-LZ	32.6±0.5 (9)	42.1±0.8 (11)	n. d. (9)	0.89±0.11 (11)

Data are expressed as mean±S.E.M. with a number of animals in parentheses.
n.d., not detectable.

3.3. Methyl-CpG status of MT2 gene altered by prenatal Zn deficiency

We hypothesized that the *MT2* mRNA abundance in IU-LZ mice is enhanced by epigenetic alterations. Then, we analyzed the DNA methylation frequency by bisulfite sequencing with a special reference to the methyl-CpG status in the *MT2* promoter region and

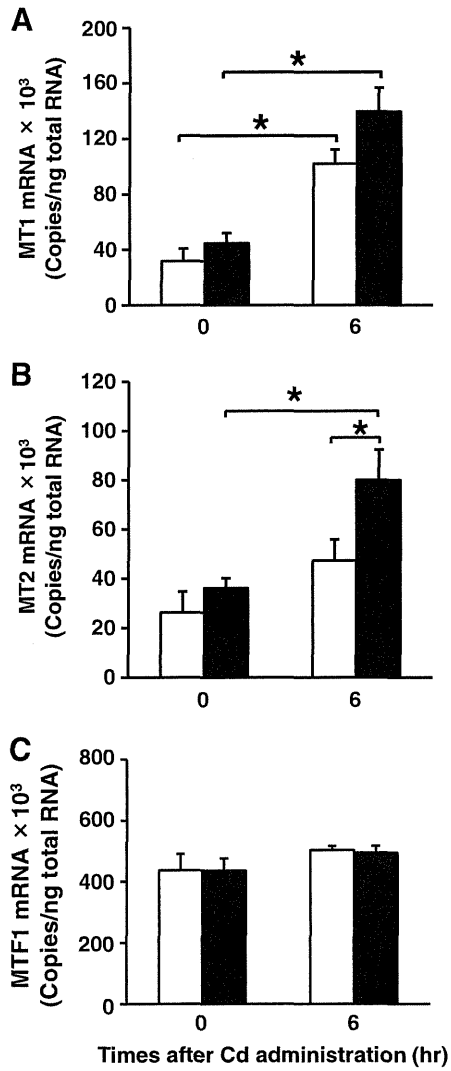

Fig. 2. Abundances of *MT1*, *MT2* and *MTF1* mRNA upon Cd exposure in liver of 5-week-old pups fed a low-Zn diet: (A) *MT1* mRNA, (B) *MT2* mRNA and (C) *MTF1* mRNA. IU-CZ (open) and IU-LZ (closed) groups. Data are expressed as mean±SEM (IU-CZ 0 h, $n=5$; IU-LZ 0 h, $n=9$; IU-CZ 6 h, $n=6$; IU-LZ 6 h, $n=11$). Statistically significant difference was determined by two-way ANOVA, followed by *post hoc* Bonferroni's test (*$P<.05$).

compared the DNA methylation frequency between IU-CZ and IU-LZ mice in 5-week-old mice. The locations of the transcription start site, MREs, TATA box, and target regions amplified by primer sets are shown in Fig. 3A. The CpG islands, from the −480 to +140 bp region (BS-R4 and BS-R5) of the *MT2* gene, which include MREs, were not methylated in IU-CZ and IU-LZ mice. Although the vast majority of CpG sites in the promoter region showed absolutely no methylation in either animal groups, the −834 and −820 bp CpG sites in IU-LZ mice were more frequently methylated than those in IU-CZ mice. Since the −820 bp CpG site (Fig. 3B; arrow) has the CCGC sequence that can be recognized by the methyl-sensitive restriction enzyme *Aci* I, methylation frequency analysis using *Aci* I was performed at the −820 CpG

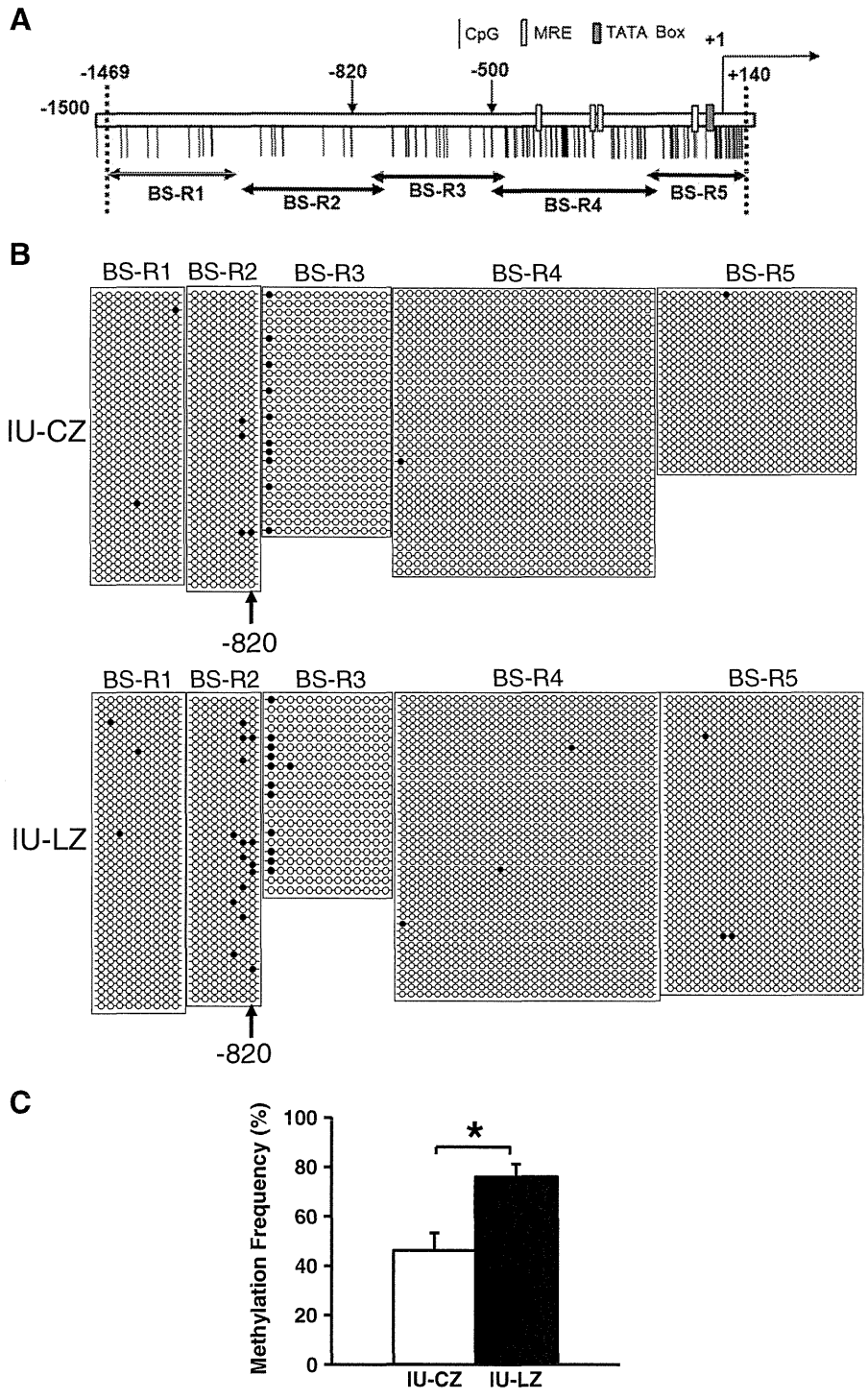

Fig. 3. Comparison of DNA methylation status and frequency of 5′-flanking region of *MT2* gene in livers of 5-week-old mice grown under perinatal Zn deficiency. (A) Target regions of *MT2* gene analyzed by bisulfite genomic sequencing. The locations of transcription start site, MREs and TATA box are shown in a previous study [50]. (B) DNA methylation status and frequency of 5′-flanking region of *MT2* of the control (IU-CZ: opened) and Zn deficiency (IU-LZ: closed) mice: CpG dinucleotides are represented by circles (●, methylated cytosine; ○, unmethylated cytosine). (C) Methylation frequency of -820 bp CpG determined by quantitative PCR with methylation-sensitive restriction enzyme. Open (IU-CZ mice) and closed (IU-LZ mice) columns are presented. Data are expressed as mean±S.E.M. (IU-CZ, $n=5$; IU-LZ, $n=9$). Statistically significant difference was determined by Student's t test (*$P<.05$).

site in the IU-CZ (n=6) and IU-LZ (n=9) mouse samples. A significant increase in DNA methylation frequency was observed at the −820 CpG site in IU-LZ mouse samples, suggesting the association of prenatal Zn deficiency with a high methylation status (Fig. 3C), which is consistent with the result of bisulfite sequencing (Fig. 3B).

3.4. MT2 promoter analysis

No data on *MT2* promoter functional analysis in various animal species is available. Thus, using an *MT2* gene-promoter-driven luciferase reporter gene assay, we confirmed that *MT2* mRNA abundances were significantly induced in Hepa1c1c7 cells as early as 3 h after Cd addition to the medium (Fig. 4A). For deletion analysis, we made six deletion constructs from an original construct connected with a 2,166 bp flanking region to the pGL4 vector (*pGL4MT2-2166*), on the basis of the strategy that the possible functionalities of the four MREs can be evaluated (Fig. 4B). Hepa1c1c7 cells that were transfected with either of the *pGL4MT2-2166, pGL4MT2-397, pGLMT2-307* or *pGLMT2-287*construct were found to have significantly elevated transcription activity upon exposure to 5.0 or 10.0 μM Cd (Fig. 4B). However, almost no additional induction above a constitutive level was observed by Cd treatment in the following three transfected cell lines: cells transfected with *pGL4MT2Δ-397-37* construct from which all four MRE motifs were deleted, those transfected with *pGL4MT2-65* having an MRE motif and those transfected with *pGL4MT2-37* having no MRE motif (Fig. 4B). Collectively, only one MRE located between a −287 to −65 bp region are suggested to play a crucial role in the induction of *MT2* mRNA by Cd in these cells.

3.5. Histone modifications of MT2 gene altered by prenatal Zn deficiency

We applied the ChIP assay to the four target regions (Ch-R1, Ch-R2, Ch-R3 and Ch-R4) of the *MT2* promoter regions, in 5-week-old mice, which contain MREs or −820 CpG, to examine whether histone modifications are altered by the Zn status in the prenatal period (Fig. 5A). We found that the basal amounts of AcH3 at Ch-R1 and Ch-R3, AcH4 at Ch-R1 and Ch-R2 and AcH3K14 at Ch-R3 in IU-LZ mice are significantly higher than those in IU-CZ mice (Fig. 5B, C and E). In Cd-exposed mice, histone modification levels in IU-LZ mice in comparison with those in IU-CZ mice were significantly increased: AcH3 (Fig. 5B) and AcH4 (Fig. 5C) levels in Ch-R2, Ch-R3, and Ch-R4; AcH3K9 (Fig. 5D) levels at Ch-R2 and Ch-R3; AcH3K14 levels in Ch-R1, Ch-R2, Ch-R3 and Ch-R4 (Fig. 5E); and H3K4me3 levels at Ch-R3 (Fig. 5F).

In IU-LZ mice, Cd administration significantly increased the AcH3K14 levels at Ch-R1 and Ch-R2 (Fig. 5E) and H3K4me3 levels at Ch-R3 (Fig. 5F), whereas it significantly decreased the AcH3 (Fig. 5B) and AcH4 (Fig. 5C) levels at Ch-R1. It is not known why Cd exposure reduced histone acetylation in the Ch-R1 region. However, this region is not considered to be responsible for transcription. Next, to determine whether these histone modifications occurred in the newborn livers, we analyzed *MT2* promoter regions in the liver from the 1-day-old pups born to dams given a Zn deficient diet during gestation. The abundances of *MT1, MT2* and *MTF1* mRNAs in IU-LZ

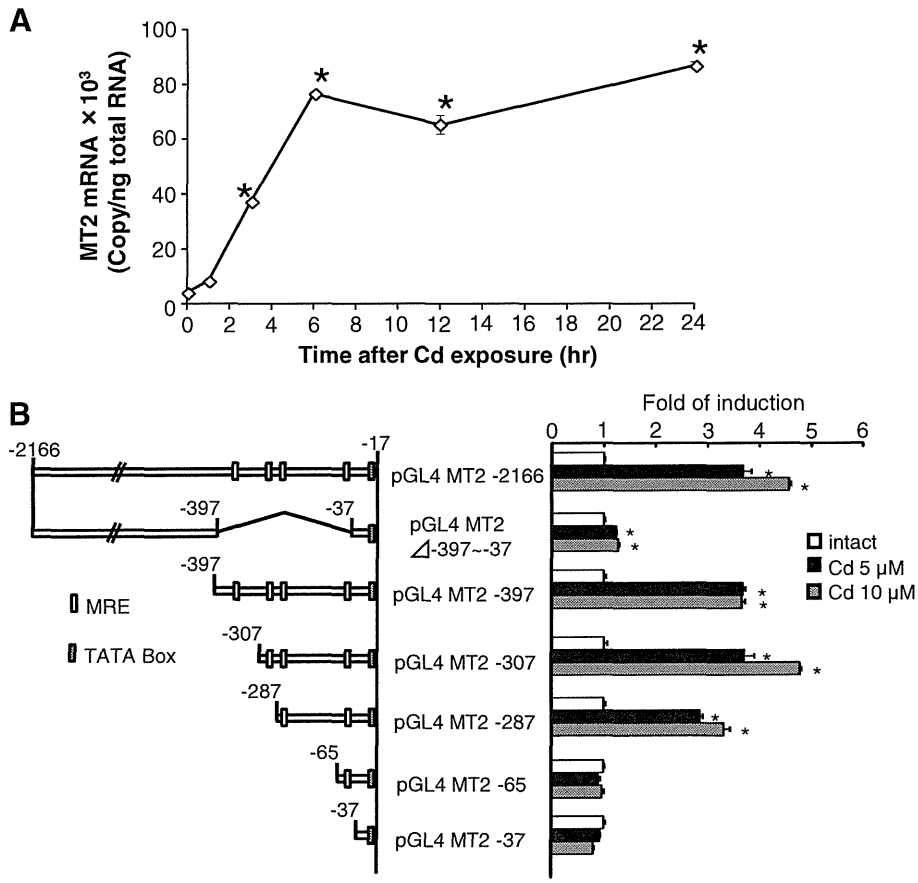

Fig. 4. *MT2* promoter analysis using reporter gene assay. (A) Abundance of *MT2* mRNA in Hepa1c1c7 cells at 0, 3, 6, 12 and 24 h after 5.0 μM Cd treatment. Data are expressed as mean±S.E.M. (*n*=3 per group). Statistically significant difference was determined by one-way ANOVA, followed by post hoc Bonferroni's test (*P<.05 vs. 0 h). (B) Structure of MT2 MRE-deletion constructs (left). Reporter gene activity in Hepa1c1c7 cells transfected with MT2 MRE-deletion constructs at 24 h after 5.0 and 10.0 μM Cd treatment (right). Data are expressed as mean±S.E.M. (*n*=3 per group). Statistically significant difference was determined by one-way ANOVA, followed by post hoc Bonferroni's test at each construct (*P<.05 vs. intact).

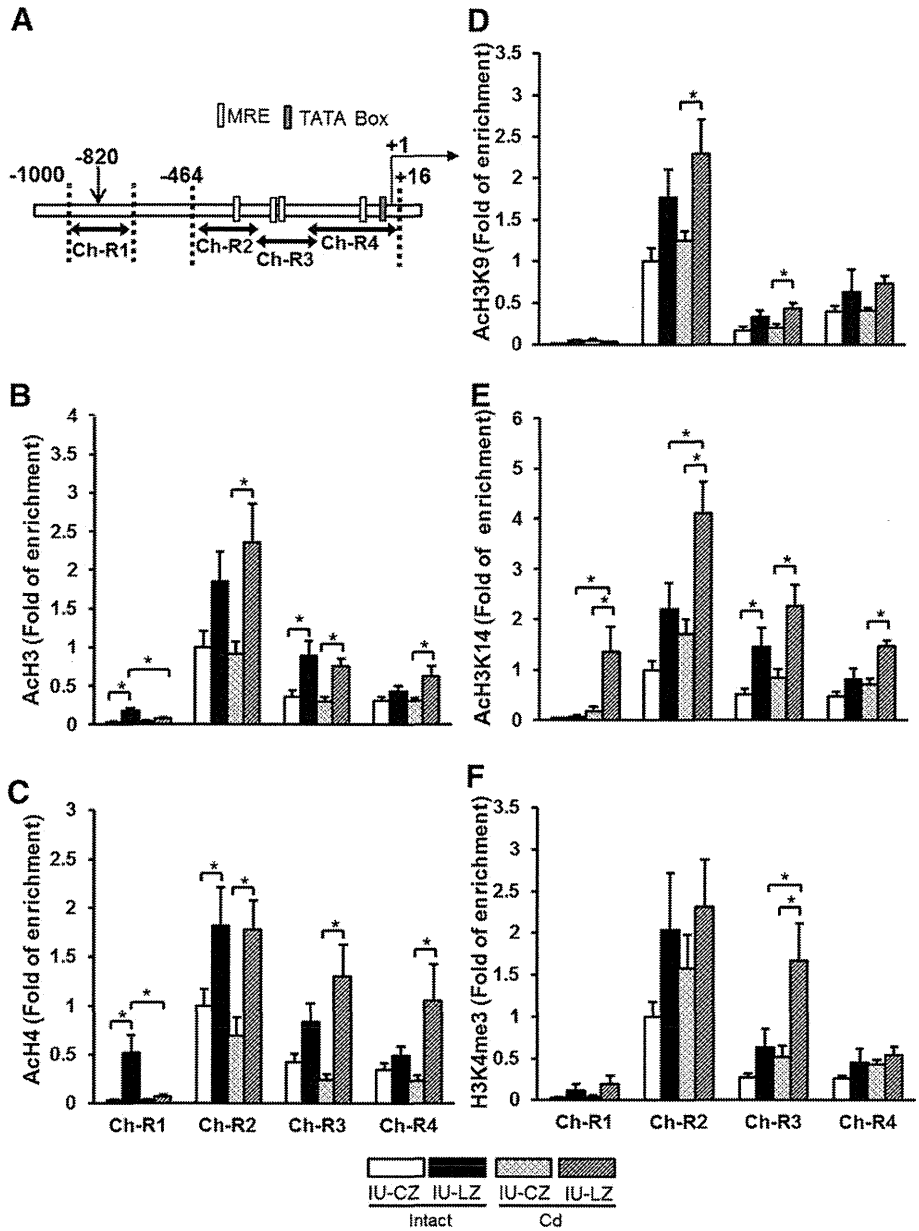

Fig. 5. Changes in histone modification levels in *MT2* promoter regions in 5-week-old mice grown under prenatal Zn deficiency. The livers were collected before and 6 h after Cd administration. (A) Target regions of *MT2* promoter for ChIP assay and localizations of transcription start site, MREs and TATA box are shown in a the previous study [50]. Changes in levels of (B) acetylated histone H3, (C) acetylated histone H4, (D) acetylated histone H3 lysine 9, (E) acetylated histone H3 lysine 14, and (F) tri-methylated histone H3 lysine 4. Open (IU-CZ intact mice), closed (IU-LZ intact mice), dotted (IU-CZ Cd-exposed mice), and diagonal (IU-LZ Cd-exposed mice) columns are presented. Data are expressed as mean±S.E.M. (n=8 per group). Statistically significant difference was determined by two-way ANOVA, followed by post hoc Bonferroni's test at each region (*P<.05).

mice was not altered in comparison with those in IU-CZ mice (Fig. 6A).The AcH3 levels at Ch-R2 and Ch-R3 were significantly higher in IU-LZ mice than in IU-CZ mice (Fig. 6B). The AcH4 levels at Ch-R2 in IU-LZ mice tended to increase in comparison with those in IU-CZ mice (Fig. 6C). These results suggest that the histone acetylation level was already initiated to increase during the perinatal stage by the Zn deficiency *in utero*.

3.6. Zn deficiency in utero prolonged MTF1 binding to the MT2 promoter region upon Cd administration

Since the epigenetic alterations as shown in the previous section suggested the loosening of the chromatin structure in the *MT2* promoter region, we investigated whether Cd exposure *in vivo* affects the status of MTF1binding to a particular region (Ch-R1, Ch-R2, Ch-R3, and Ch-R4) in the *MT2* promoter by the ChIP assay (Table 2). The amounts of MTF1 bound to Ch-R2, Ch-R3 and Ch-R4 were greater at 1 h than those at 0 and 6 h after Cd administration in all the animals (Table 2). The amount of MTF1 bound to Ch-R1, which does not have an MRE motif, was not detected at these time points (data not shown).

The amounts of MTF1bound to Ch-R3 and Ch-R4, but not Ch-R2 were observed to be significantly higher in IU-LZ mice than in IU-CZ mice 6 h after Cd administration, whereas no difference in the amounts of MTF1 bound to these regions was found between the IU-CZ and IU-LZ mice 1 h after Cd administration, which suggests the prolongation of MTF1 binding to the MRE motif (Table 2). The amounts of MTF1 protein in both nucleus and cytosol were unchanged between the IU-LZ and IU-CZ mice and between before

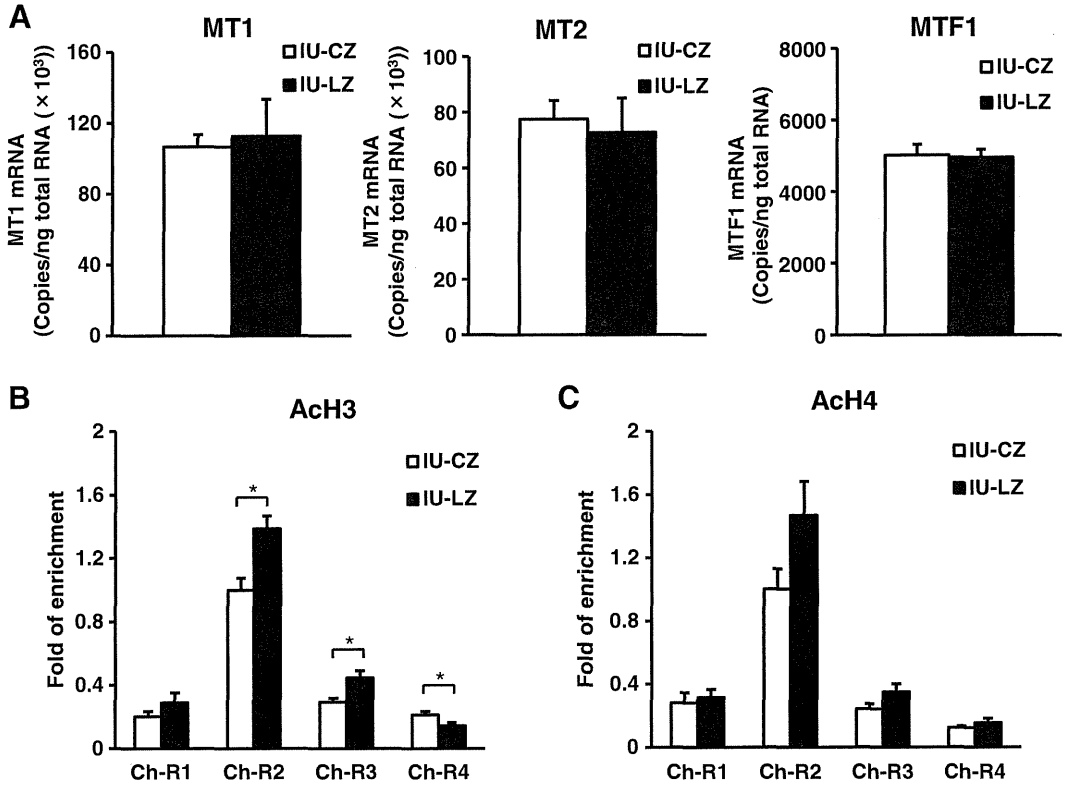

Fig. 6. (A) Abundances of *MT1*, *MT2* and *MTF1* mRNAs and (B) levels of acetylated histone H3 and (C) histone H4 in the *MT2* gene in the liver in 1-day-old male pups grown under Zn deficiency condition. The target regions for histone modifications analysis are shown in Fig. 5A. Data are expressed as mean±S.E.M. (n=6 per group). Statistically significant difference was determined by Student's t test at each region (*P<.05).

and 6 h after Cd administration (Fig. 7), suggesting that the total amounts of MTF1 protein in the liver were not altered by prenatal Zn deficiency or Cd administration.

3.7. Epigenetic alterations induced by Zn-deficiency in adulthood

To determine whether the epigenetic alterations induced by Zn deficiency are a temporally specific event, adult mice were fed a low-Zn diet or a control diet for 12 days, and the liver was collected just after the end of this period and subjected to the epigenetic analyses. In the AD-CZ and AD-LZ mice, no significant differences in the mRNA abundances of *MT1*, *MT2* and *MTF1* were found (Fig. 8A).Although the levels of AcH3 (Fig. 8B) and AcH3K14 (Fig. 8E) at Ch-R1 in the *MT2* promoter of AD-LZ mice were significantly higher than those of AD-CZ mice, the differences were not conspicuous. No significant differences in the amounts of other histone modifications in AcH4 (Fig. 8C), AcH3K9 (Fig. 8D) and H3K4me3 (Fig. 8F) were found between AD-LZ and AD-CZ mice. In addition, the DNA methylation frequency at a −820 bp CpG site in the *MT2* promoter of AD-LZ mice was not different from that of the AD-CZ mice (Fig. 8G).

Next, to study the possible involvement of Zn deficiency in the inducibilities of *MT1/2* mRNAs, the Zn-deficient diet was replaced with a regular diet, and the inducibilities of *MT1* and *MT2* mRNAs by Cd administration were examined one month later. Under this condition, no difference in *MT1* and *MT2* mRNA abundances was observed between the AD-LZ and AD-CZ mice 6 h after Cd administration (Fig. 8H). The *MTF1* mRNA abundance was significantly lower in AD-LZ mice than in the AD-CZ mice (Fig. 8I).

Collectively, epigenetic alterations of the *MT2* gene were found to be caused by Zn deficiency during the prenatal period, but not in adulthood.

4. Discussion

A remarkable finding of this study is that epigenetic alterations of the promoter of the *MT2* gene under prenatal Zn deficiency condition are associated with a significant enhancement of Cd-dependent induction of *MT2* mRNA in the liver of mouse progeny later in adulthood. The first question that was addressed is when such epigenetic alterations occur and how long they last. In the 5-week-old

Table 2
Amounts of MTF1 bound to MT2 promoter post Cd administration in the liver of 5-week-old mice born to dams fed a low-Zn diet or a control diet

Target region	Ch-R2			Ch-R3			Ch-R4		
Time post Cd administration (h)	0	1	6	0	1	6	0	1	6
	Fold of enrichment								
IU-CZ	1.00±0.29	9.13±3.44	0.74±0.23	1.00±0.45	6.21±1.60	0.65±0.18	1.00±0.31	3.24±1.08	0.32±0.06
IU-LZ	0.69±0.25	9.17±2.76	0.45±0.10	0.54±0.20	8.00±3.69	1.54±0.25*	0.78±0.19	3.30±1.25	1.16±0.30*

Each target regions are the ones shown in Fig. 5A. Data are expressed as mean±S.E.M. (n=6 per group).
Statistically significant difference between IU-CZ and IU-LZ mice by Student's t-test (*P<.05).

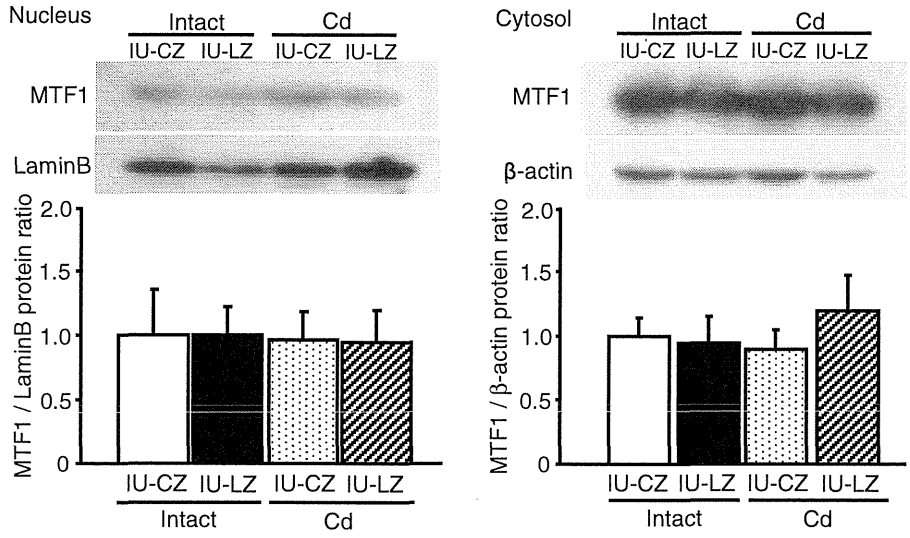

Fig. 7. Amounts of hepatic MTF1 protein in 5-week-old pups grown under Zn deficiency condition. The livers were collected before and 6 h after Cd administration. Scanning densitometry was used for semi quantitative analysis. Data are expressed as mean±S.E.M. (n=5 per group).

IU-LZ mice, significant increases in DNA methylation frequency at the −820 CpG site and histone modifications were demonstrated in comparison with those in IU-CZ mouse progeny. However, this region is not considered to be responsible for transcription. To examine when these histone modifications were caused by Zn deficiency, we analyzed the *MT2* promoter region in the liver from the 1-day-old pups born to dams given a Zn-deficient diet during gestation. Collectively, the IU-LZ mice had significantly elevated AcH3 levels at Ch-R2 and Ch-R3 and showed a tendency of AcH4 levels to increase at Ch-R2 in comparison with IU-CZ mice, suggesting that histone acetylation levels were increased during the prenatal stage. Taken together, zinc deficiency *in utero* alters fetal histone modifications, and these changes are being stored as an epigenetic memory until adulthood (Supplemental Fig. 1). In this study, we could not provide direct evidence on molecular mechanisms by which histone modification enhance Cd-induced *MT2* mRNA expression in IU-LZ mice. However, the elevation in histone acetylation observed in the IU-LZ mice is considered to keep the nucleosome in an "open chromatin" state [38]. Therefore, it is likely that p300 and Sp1 that are known to be recruited by MTF1 [30] will easily make an access to the *MT2* promoter region under the open chromatin condition and that Cd-induced *MT2* mRNA abundance is enhanced in IU-LZ mice. Further studies will be required to reveal the molecular mechanisms how prenatal Zn deficiency regulates not only gene expression via histone modifications, but also maintain histone modifications.

The next question was whether the epigenetic alterations are more specifically induced by Zn deficiency *in utero* rather than in adulthood. When adult mice fed a low-Zn diet (AD-LZ) or those fed a control diet (AD-CZ) were compared, the levels of AcH3/AcH3K14 of the *MT2* gene at Ch-R1 in AD-LZ mice were significantly different from those in AD-CZ mice. However, these changes did not seem to contribute to the alteration of the induction of *MT2* transcription following Cd exposure, because the Ch-R1 region is considered to be irrelevant to transcription (Fig. 4). In addition, the induction of *MT2* mRNA by Cd exposure in AD-LZ mice was not different from that in AD-CZ mice (Fig. 8H). Therefore, it is not likely that the alteration of histone modifications induced by Zn deficiency played a significant role to induce *MT2* mRNA upon Cd exposure in AD-LZ mice. Our results clearly show that mouse fetuses are more responsive to Zn deficiency resulting in epigenetic alterations than adult mice. On the other hand, epigenetic alterations are known to be caused by environmental factors in adulthood as well. Examples of this are an increase in DNA methylation levels of tumor-suppressor genes, such as p16, in the stomach following infection by *Helicobacter pylori* in humans [39,40], DNA hypomethylation of *Pparγ* in mice fed a high-fat diet [41] and DNA hypermethylation of *PPIc* and DNA hypomethylation of *fosB* in nucleus accumbens in cocaine-administered mice [42]. In the case of the nutritional status of Zn, significant epigenetic alterations might occur when adult animals are exposed to extremely low Zn levels for a longer time than under the present experimental conditions.

The other question is how Cd administration enhanced the *MT2* induction in IU-LZ mice compared with IU-CZ mice later in life. A plausible explanation is that the prenatal Zn deficiency induced enhanced histone modifications in the *MT2* promoter region that includes MREs, and that MTF1 or yet-unidentified transcription factors may have easy access to the MRE motif to activate the *MT2* gene expression upon Cd or Zn exposure. This conjecture was supported by the elevated levels of acetylated histones and methylated H3K4 in the *MT2*-400 bp 5′ flanking region in the IU-LZ mice compared with those in the IU-CZ mice (Fig. 5). It is reasonable to think that such an open-chromatin structure persists into adulthood and allows transcription to be activated, as has been reported for other genes such as *Hoxa10* or *Gfap* [43,44].On the other hand, because of the lack of MRE motifs, it is less likely that the change in DNA methylation frequency at −820 bp CpG in the *MT2* promoter region in the IU-LZ mice is associated with the enhanced *MT2* gene expression later in life (Fig. 3).

MTF1 binding to the MRE motif in the *MT1* gene has been proposed to play an important role in the induction of this gene [30]. Although no data are available on the interaction of MTF1 with the *MT2* gene, our reporter gene assay (Fig. 4) and ChIP assay (Table 2) results suggested that MTF1 can bind to the MRE motif in the *MT2* gene. The significantly prolonged MTF1 binding 6 h after Cd administration in the IU-LZ mice (Table 2) may explain the enhanced *MT2* mRNA induction: That is, it is conceivable that the highly acetylated state of histones bound to the DNA fragment adjacent to MREs (Fig. 5) affects the three-dimensional interaction between the MTF1 protein and DNA, and that the net dissociation of MRE with MTF1 may be reduced owing to structural changes in the nucleosome. As described above, the possible removal or slide of histone H3 in *MT1* promoter by Zn treatment may have an interaction with MTF1, and the binding of MTF1 to the promoter is required to initiate the exclusion of histone [45]. Thus, it can be speculated that the

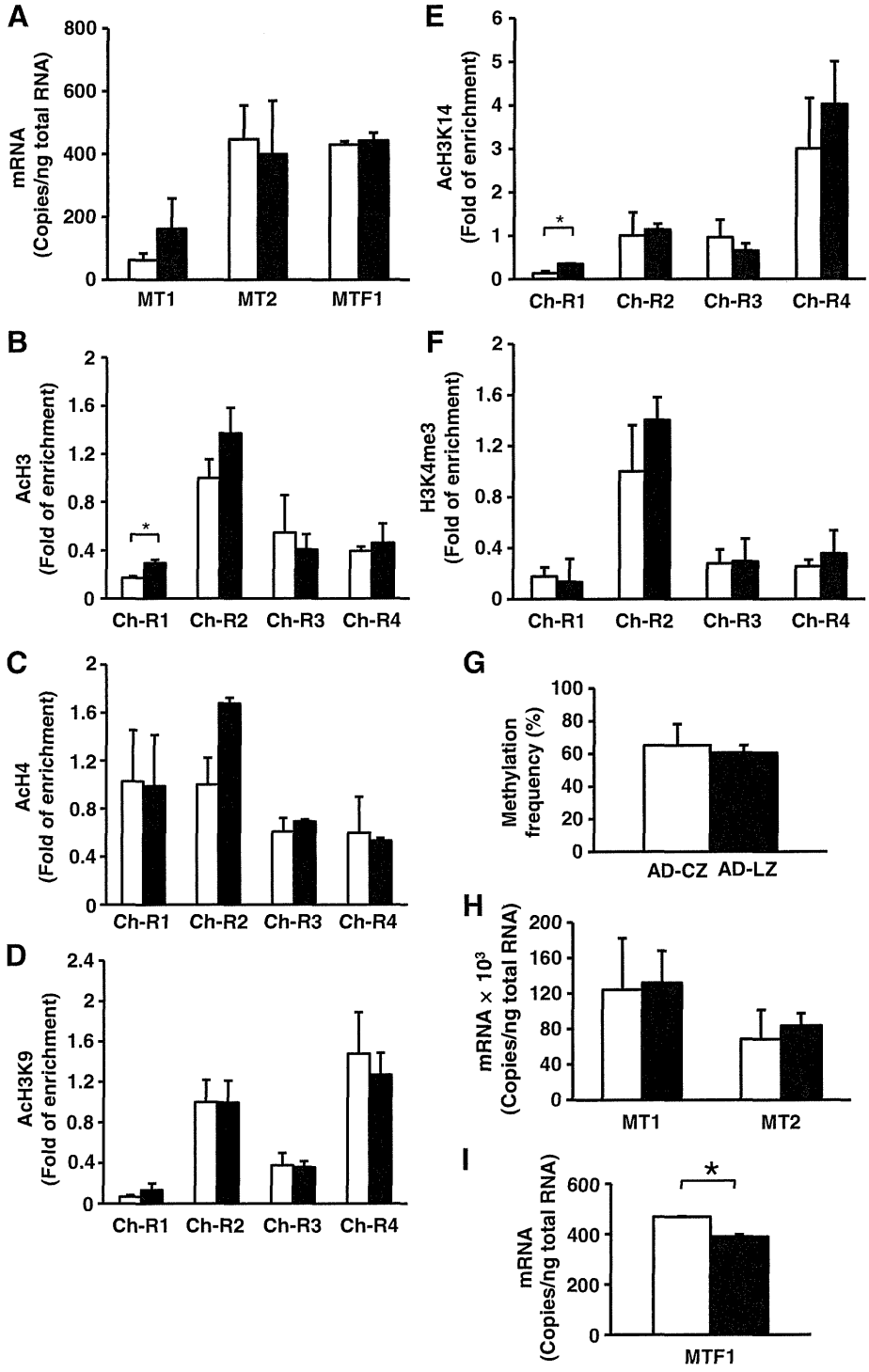

Fig. 8. Abundances of *MT1*, *MT2* and *MTF1* mRNAs, and histone modification in the *MT2* promoter of liver from mice fed a low-Zn diet for 12 days in adulthood (A-G), or those fed with a low-Zn diet followed by a regular diet for a month in adulthood (H-I). (A) *MT1*, *MT2* and *MTF1* mRNAs. (B) Acetylated histone H3. (C) Acetylated histone H4. (D) Acetylated histone H3 lysine 9. (E) Acetylated histone H3 lysine 14. (F) Tri-methylated histone H3 lysine 4. (G) Methylation frequency of −820 bp CpG included in *Aci* I site. See legend to Fig. 5A for target regions of histone modifications. Data on hepatic *MT1* and *MT2* (H) and *MTF1* mRNA (I) were obtained 6 h after oral administration of Cd at 5.0 mg kg^{-1} b.w. Open (AD-CZ mice) and closed (AD-LZ mice) columns are presented. Data are expressed as mean±S.E.M. ($n=3$ per group). Statistically significant difference was determined by Student's *t* test (*$P<.05$).

prolonged binding of MTF1 to *MT2* promoter in IU-LZ mice may be involved in the maintenance of the opened chromatin structure.

Another question to be addressed is what the enhanced *MT2* mRNA induction in adulthood caused by *in utero* Zn deficiency indicates. It has been reported that abnormal morphogenesis occurred in the *MT1/2*-null fetus grown under Zn deficiency *in utero* [46]. On the contrary, this effect was prevented in the transgenic mice over expressing the MT1 protein [47]. *MT1/2* null mice fed a low-Zn diet for 3 weeks from birth developed swollen Bowman's space in the kidney in comparison with wild-type mice [48]. These studies suggest that MT1/2 proteins protect against Zn deficiency. It can be speculated from our study that mice grown under prenatal Zn deficiency maintain the inducibility of *MT2* mRNA as an epigenetic memory in the genome. In this case, it is thought that mice can be prepared for Zn

deficiency that they may encounter in the future, and that they will be able to efficiently response to the low-Zn condition. This idea could be supported by an analogy to the thrifty phenotype hypothesis in that neonates who experienced poor nutrition *in utero* have metabolic adaptations that emerge in anticipation of a low-quality adult breeding environment [49].

In conclusion, the present study demonstrates for the first time that prenatal Zn deficiency causes epigenetic alterations in the liver of offspring. The enhanced *MT2* gene induction by metal exposure after birth is considered to be due to epigenetic alterations, such as enhanced acetylation levels of histones bound to approximately −400 bp of the *MT2*-5′flanking region. Histone modifications caused by Zn deficiency during the early-developmental period may persist into adulthood as an epigenetic memory. The results of the present study results could also support the DOHaD hypothesis from the perspective that a particular nutrition factor such as an essential trace element during prenatal period can affect epigenome of children.

Acknowledgments

We thank Dr. Chiho Watanabe (Department of Human Ecology, Graduate School of Medicine, The University of Tokyo) for useful suggestions on the result of our experiments, and colleagues in our laboratory for constructive comments.

Appendix A. Supplementary data

Supplementary data to this article can be found online at http://dx.doi.org/10.1016/j.jnutbio.2012.05.013.

References

[1] Painter RC, Roseboom TJ, Bleker OP. Prenatal exposure to the Dutch famine and disease in later life: an overview. Reprod Toxicol 2005;20:345–52.
[2] Barker DJ, Winter PD, Osmond C, Margetts B, Simmonds SJ. Weight in infancy and death from ischaemic heart disease. Lancet 1989;2:577–80.
[3] Barker DJ, Osmond C, Golding J, Kuh D, Wadsworth ME. Growth in utero, blood pressure in childhood and adult life, and mortality from cardiovascular disease. BMJ 1989;298:564–7.
[4] Forsen T, Eriksson JG, Tuomilehto J, Osmond C, Barker DJ. Growth in utero and during childhood among women who develop coronary heart disease: longitudinal study. BMJ 1999;319:1403–7.
[5] Gillman MW, Barker D, Bier D, Cagampang F, Challis J, Fall C, et al. Meeting report on the 3rd International Congress on Developmental Origins of Health and Disease (DOHaD). Pediatr Res 2007;61:625–9.
[6] Torrens C, Poston L, Hanson MA. Transmission of raised blood pressure and endothelial dysfunction to the F2 generation induced by maternal protein restriction in the F0, in the absence of dietary challenge in the F1 generation. Br J Nutr 2008;100:760–6.
[7] Burdge GC, Slater-Jefferies J, Torrens C, Phillips ES, Hanson MA, Lillycrop KA. Dietary protein restriction of pregnant rats in the F0 generation induces altered methylation of hepatic gene promoters in the adult male offspring in the F1 and F2 generations. Br J Nutr 2007;97:435–9.
[8] Simmons RA, Templeton LJ, Gertz SJ. Intrauterine growth retardation leads to the development of type 2 diabetes in the rat. Diabetes 2001;50:2279–86.
[9] Park JH, Stoffers DA, Nicholls RD, Simmons RA. Development of type 2 diabetes following intrauterine growth retardation in rats is associated with progressive epigenetic silencing of Pdx1. J Clin Invest 2008;118:2316–24.
[10] Bernal AJ, Jirtle RL. Epigenomic disruption: the effects of early developmental exposures. Birth Defects Res A Clin Mol Teratol 2010;88:938–44.
[11] Newbold RR, Padilla-Banks E, Jefferson WN, Heindel JJ. Effects of endocrine disruptors on obesity. Int J Androl 2008;31:201–8.
[12] Waterland RA, Travisano M, Tahiliani KG. Diet-induced hypermethylation at agouti viable yellow is not inherited transgenerationally through the female. FASEB J 2007;21:3380–5.
[13] Jones PA, Baylin SB. The fundamental role of epigenetic events in cancer. Nat Rev Genet 2002;3:415–28.
[14] Jenuwein T, Allis CD. Translating the histone code. Science 2001;293:1074–80.
[15] Anway MD, Cupp AS, Uzumcu M, Skinner MK. Epigenetic transgenerational actions of endocrine disruptors and male fertility. Science 2005;308:1466–9.
[16] Tomat AL, Inserra F, Veiras L, Vallone MC, Balaszczuk AM, Costa MA, et al. Moderate zinc restriction during fetal and postnatal growth of rats: effects on adult arterial blood pressure and kidney. Am J Physiol Regul Integr Comp Physiol 2008;295:R543–9.
[17] Halas ES, Eberhardt MJ, Diers MA, Sandstead HH. Learning and memory impairment in adult rats due to severe zinc deficiency during lactation. Physiol Behav 1983;30:371–81.
[18] Halas ES, Hunt CD, Eberhardt MJ. Learning and memory disabilities in young adult rats from mildly zinc deficient dams. Physiol Behav 1986;37:451–8.
[19] Beach RS, Gershwin ME, Hurley LS. Gestational zinc deprivation in mice: persistence of immunodeficiency for three generations. Science 1982;218:469–71.
[20] Tuerk MJ, Fazel N. Zinc deficiency. Curr Opin Gastroenterol 2009;25:136–43.
[21] Vallee BL, Falchuk KH. The biochemical basis of zinc physiology. Physiol Rev 1993;73:79–118.
[22] Hunt JR. Bioavailability of iron, zinc, and other trace minerals from vegetarian diets. Am J Clin Nutr 2003;78:633S–9S.
[23] Wastney ME, Ahmed S, Henkin RI. Changes in regulation of human zinc metabolism with age. Am J Physiol 1992;263:R1162–8.
[24] Menzano E, Carlen PL. Zinc deficiency and corticosteroids in the pathogenesis of alcoholic brain dysfunction — a review. Alcohol Clin Exp Res 1994;18:895–901.
[25] Jeejeebhoy K. Zinc: an essential trace element for parenteral nutrition. Gastroenterology 2009;137:S7–12.
[26] Fischer Walker CL, Ezzati M, Black RE. Global and regional child mortality and burden of disease attributable to zinc deficiency. Eur J Clin Nutr 2009;63:591–7.
[27] Coyle P, Philcox JC, Carey LC, Rofe AM. Metallothionein: the multipurpose protein. Cell Mol Life Sci 2002;59:627–47.
[28] Nies DH. Microbial heavy-metal resistance. Appl Microbiol Biotechnol 1999;51:730–50.
[29] Solis WA, Childs NL, Weedon MN, He L, Nebert DW, Dalton TP. Retrovirally expressed metal response element-binding transcription factor-1 normalizes metallothionein-1 gene expression and protects cells against zinc, but not cadmium, toxicity. Toxicol Appl Pharmacol 2002;178:93–101.
[30] Li Y, Kimura T, Huyck RW, Laity JH, Andrews GK. Zinc-induced formation of a coactivator complex containing the zinc-sensing transcription factor MTF-1, p300/CBP, and Sp1. Mol Cell Biol 2008;28:4275–84.
[31] Vruwink KG, Hurley LS, Gershwin ME, Keen CL. Gestational zinc deficiency amplifies the regulation of metallothionein induction in adult mice. Proc Soc Exp Biol Med 1988;188:30–4.
[32] Tomat AL, Inserra F, Veiras L, Vallone MC, Balaszczuk AM, Costa MA, et al. Moderate zinc restriction during fetal and postnatal growth of rats: effects on adult arterial blood pressure and kidney. Am J Physiol Regul Integr Comp Physiol 2008;295:R543–9.
[33] Wang FD, Bian W, Kong LW, Zhao FJ, Guo JS, Jing NH. Maternal zinc deficiency impairs brain nestin expression in prenatal and postnatal mice. Cell Res 2001;11:135–41.
[34] Oteiza PI, Hurley LS, Lonnerdal B, Keen CL. Marginal zinc deficiency affects maternal brain microtubule assembly in rats. J Nutr 1988;118:735–8.
[35] Shiizaki K, Ohsako S, Koyama T, Nagata R, Yonemoto J, Tohyama C. Lack of CYP1A1 expression is involved in unresponsiveness of the human hepatoma cell line SK-HEP-1 to dioxin. Toxicol Lett 2005;160:22–33.
[36] Clark SJ, Harrison J, Paul CL, Frommer M. High sensitivity mapping of methylated cytosines. Nucleic Acids Res 1994;22:2990–7.
[37] Lee TI, Johnstone SE, Young RA. Chromatin immunoprecipitation and microarray-based analysis of protein location. Nat Protoc 2006;1:729–48.
[38] Kouzarides T. Chromatin modifications and their function. Cell 2007;128:693–705.
[39] Maekita T, Nakazawa K, Mihara M, Nakajima T, Yanaoka K, Iguchi M, et al. High levels of aberrant DNA methylation in Helicobacter pylori-infected gastric mucosae and its possible association with gastric cancer risk. Clin Cancer Res 2006;12:989–95.
[40] Nakajima T, Maekita T, Oda I, Gotoda T, Yamamoto S, Umemura S, et al. Higher methylation levels in gastric mucosae significantly correlate with higher risk of gastric cancers. Cancer Epidemiol Biomarkers Prev 2006;15:2317–21.
[41] Fujiki K, Kano F, Shiota K, Murata M. Expression of the peroxisome proliferator activated receptor gamma gene is repressed by DNA methylation in visceral adipose tissue of mouse models of diabetes. BMC Biol 2009;7:38.
[42] Anier K, Malinovskaja K, Aonurm-Helm A, Zharkovsky A, Kalda A. DNA methylation regulates cocaine-induced behavioral sensitization in mice. Neuropsychopharmacology 2010;35:2450–61.
[43] Bromer JG, Zhou Y, Taylor MB, Doherty L, Taylor HS. Bisphenol-A exposure in utero leads to epigenetic alterations in the developmental programming of uterine estrogen response. FASEB J 2010;24:2273–80.
[44] Asano H, Aonuma M, Sanosaka T, Kohyama J, Namihira M, Nakashima K. Astrocyte differentiation of neural precursor cells is enhanced by retinoic acid through a change in epigenetic modification. Stem Cells 2009;27:2744–52.
[45] Okumura F, Li Y, Itoh N, Nakanishi T, Isobe M, Andrews GK, et al. The zinc-sensing transcription factor MTF-1 mediates zinc-induced epigenetic changes in chromatin of the mouse metallothionein-I promoter. Biochim Biophys Acta 2011;1809:56–62.
[46] Andrews GK, Geiser J. Expression of the mouse metallothionein-I and -II genes provides a reproductive advantage during maternal dietary zinc deficiency. J Nutr 1999;129:1643–8.
[47] Dalton T, Fu K, Palmiter RD, Andrews GK. Transgenic mice that overexpress metallothionein-I resist dietary zinc deficiency. J Nutr 1996;126:825–33.
[48] Kelly EJ, Quaife CJ, Froelick GJ, Palmiter RD. Metallothionein I and II protect against zinc deficiency and zinc toxicity in mice. J Nutr 1996;126:1782–90.
[49] Wells JC. The thrifty phenotype hypothesis: thrifty offspring or thrifty mother? J Theor Biol 2003;221:143–61.
[50] Searle PF, Davison BL, Stuart GW, Wilkie TM, Norstedt G, Palmiter RD. Regulation, linkage, and sequence of mouse metallothionein I and II genes. Mol Cell Biol 1984;4:1221–30.

NeuroToxicology 33 (2012) 1375–1380

Contents lists available at SciVerse ScienceDirect

NeuroToxicology

Effect of low-dose thalidomide on dopaminergic neuronal differentiation of human neural progenitor cells: A combined study of metabolomics and morphological analysis

Xian-Yang Qin [a,b], Hiromi Akanuma [a], Feifei Wei [c], Reiko Nagano [a], Qin Zeng [a], Satoshi Imanishi [d], Seiichiroh Ohsako [d], Jun Yoshinaga [b], Junzo Yonemoto [a], Masaru Tanokura [c], Hideko Sone [a,*]

[a] Health Risk Research Section, National Institute for Environmental Studies, 16-2 Onogawa, Tsukuba, Ibaraki 305-8606, Japan
[b] Department of Environmental Studies, Graduate School of Frontier Science, The University of Tokyo, 5-1-5 Kashiwanoha, Kashiwa, Chiba 270-8563, Japan
[c] Department of Applied Biological Chemistry, Graduate School of Agricultural and Life Sciences, The University of Tokyo, 1-1-1 Yayoi, Bunkyo-ku, Tokyo 113-8657, Japan
[d] Center for Disease Biology and Integrative Medicine, Graduate School of Medicine, The University of Tokyo, 7-3-1 Hongo, Bunkyo-ku, Tokyo 113-0033, Japan

ARTICLE INFO

Article history:
Received 17 February 2012
Accepted 31 August 2012
Available online 7 September 2012

Keywords:
Thalidomide
Dopamine
Metabolomics
Neuronal differentiation
CE-TOFMS

ABSTRACT

Thalidomide is increasingly used in anticancer and anti-inflammation therapies. However, it is known for its teratogenicity and ability to induce peripheral neuropathy, although the mechanisms underlying its neurological effect in humans are unclear. In this study, we investigated the effect of thalidomide on the metabolism and neuronal differentiation of human neural progenitor cells. We found that levels of tyrosine, phenylalanine, methionine and glutathione, which are involved in dopamine and methionine metabolism, were decreased following thalidomide treatment. Morphological analysis revealed that treatment with 100 nM thalidomide, which is much lower than clinical doses, significantly decreased the number of dopaminergic (tyrosine hydroxylase-positive) neurons, compared with control cells. Our results suggest that these adverse neurological effects of thalidomide should be taken into consideration prior to its use for the treatment of neurodegenerative and other diseases.

1. Introduction

A number of neurodegenerative diseases, including Parkinson's disease (PD), are characterized by the progressive loss of dopaminergic neurons in the substantia nigra and their projections to the striatum, which leads to various motor deficits (Ebert et al., 2008; Jeon et al., 2010). Human neural progenitor cells (hNPCs), which are capable of dividing and differentiating into many cells types of the nervous system including neurons, astrocytes and oligodendrocytes, can respond to environmental demands by increasing their proliferation and differentiation (Ryu et al., 2009). Transplantation of genetically modified hNPCs to replace and protect dopaminergic neurons, as a potential therapeutic strategy for the treatment of PD, has become increasingly popular among researchers (Kitiyanant et al., 2011; Lunn et al., 2011; Ryu et al., 2009). Furthermore, hNPCs have recently been proposed as a powerful model system for developmental neurotoxicity testing, as they have the capacity to differentiate into any cell type in the nervous system. The use of hNPCs also affords better predictive power, as there is no need to extrapolate results obtained with non-human species (Breier et al., 2008, 2010).

Thalidomide was used as a sedative drug to treat morning sickness in pregnant women in the 1950s, but was subsequently withdrawn from the market in 1961 because of severe teratogenicity and neurotoxicity (Franks et al., 2004; Lenz, 1988; Matthews and McCoy, 2003). Interestingly, subsequent studies on the mechanisms of thalidomide teratogenicity revealed that the compound was an effective anticancer and anti-inflammatory agent. The US Food and Drug Administration approved thalidomide for the treatment of lepromatous leprosy and multiple myeloma in 1998 and 2006, respectively (Kim and Scialli, 2011; Teo et al., 2005; Uhl et al., 2006). However, major obstacles to the use of thalidomide are its diverse neurological side effects.

It has been hypothesized that impairment of energy metabolism might contribute to nerve cell death in neurodegenerative diseases (Beal et al., 1993). Dysregulation of metabolites in the methionine (Met) transmethylation and transsulfuration pathways has been implicated in several neurodevelopmental diseases,

Abbreviations: CE-TOFMS, capillary electrophoresis time-of-flight mass spectrometry; DoD, day of differentiation; GSH, glutathione; HCA, hierarchical clustering analysis; hNPCs, human neural progenitor cells; MAP2, microtubule-associated protein 2; Met, methionine; PCA, principal component analysis; PD, Parkinson's disease; Phe, phenylalanine; TH, tyrosine hydroxylase; Tyr, tyrosine.

* Corresponding author. Tel.: +81 29 850 2464; fax: +81 29 850 2546.
E-mail address: hsone@nies.go.jp (H. Sone).

0161-813X/$ – see front matter © 2012 Elsevier Inc. All rights reserved.
http://dx.doi.org/10.1016/j.neuro.2012.08.016

such as PD and autism (Glaser et al., 2005; James et al., 2004). However, little is known of the effect of thalidomide on the pathogenesis of neurodegenerative diseases. It is likely that further investigation of thalidomide's mechanism of action will provide a rational basis for the development of effective and safe thalidomide-based therapies for the treatment of neurodegenerative and other diseases.

In the present study, we investigated the effect of thalidomide on dopaminergic neuronal differentiation of hNPCs using a combination of metabolomics and morphological analysis. Metabolomics of hNPCs has recently been described as a novel approach for biomarker discovery for human neurological diseases (Maletic-Savatic et al., 2008). Here, we report for the first time that thalidomide at concentrations much lower than clinical doses might impair dopamine and Met metabolic pathways and inhibit dopaminergic neuronal differentiation of hNPCs.

2. Materials and methods

2.1. Chemicals

Dimethyl sulfoxide (DMSO) was obtained from Sigma–Aldrich Co. (St. Louis, MO). Thalidomide was obtained from Wako Pure Chemicals (Osaka, Japan). DMSO was used as the primary solvent for all chemicals, and the DMSO solutions were further diluted in cell culture media for treatments. The final concentrations of DMSO in the media did not exceed 0.1% (v/v).

2.2. Cell culture and differentiation

The hNPCs, derived from H9 human embryonic stem cells, were obtained from Chemicon-Millipore (ENStem Human Neural Progenitor Expansion Kit; Norcross, GA). This cell line forms an adherent cell monolayer and can readily differentiate into different neuronal subtypes (Shin et al., 2005). On the first day of differentiation (DoD0), cells were cultured on a coating of 0.54 μg/cm^2 Laminin-511 (BioLaminaAB, Stockholm, Sweden) in 90-mm dishes (1.2 × 10^6 cells/dish) or 24-well plates (5 × 10^4 cells/well). The cells were cultured in neural differentiation medium containing phenol red-free neurobasal medium, 1× B27, 1× N2, 10 ng/ml BDNF (Invitrogen, Carlsbad, CA), and 2 mM glutamine (Sigma–Aldrich). The medium was replaced every 3 days. The cells were exposed to 0.1% DMSO or thalidomide (100 nM) during DoD3–5 and isolated for morphological analysis or metabolite analysis on DoD12 (Fig. 1).

2.3. Sample preparation for metabolite analysis

On DoD12, differentiated cells (approximately 1 × 10^7 cells/dish in triplicate) were washed twice with 5% mannitol solution to remove residual medium. Excess mannitol solution was removed via two rounds of centrifugation at maximum speed, and then 1.3 ml methanol solution containing 10 μM internal standards was added. Cells were collected using a cell scraper and the cell pellet was stored at −80 °C for subsequent extraction. Metabolome extraction was then performed as previously described (Ohashi et al., 2008). Metabolic profiling was initially performed using a single sample, and then the effect of thalidomide on target metabolites involved in dopamine and Met metabolic pathways was verified using four independent culture experiments.

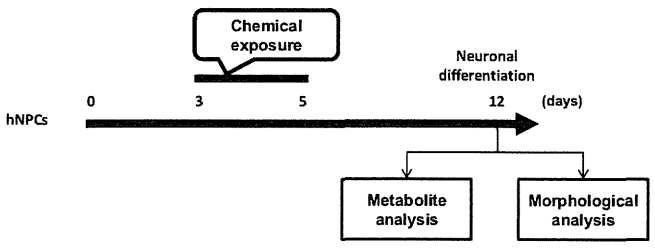

Fig. 1. Schematic overview of experimental procedures. Cells were exposed to thalidomide at a concentration of 100 nM or 10 μM during DoD3–5, and the subsequent effects on cellular metabolism and morphology were examined on DoD12.

2.4. Capillary electrophoresis time-of-flight mass spectrometry (CE-TOFMS)

Metabolic changes in response to thalidomide were examined during the neural differentiation of hNPCs using a CE-TOFMS-based metabolomics technique. This approach has been described as a sensitive, selective and rapid analytical method for anionic species, suitable for single-cell metabolomics (Lapainis et al., 2009; Ohashi et al., 2008; Soga et al., 2002). CE-TOFMS was performed using an Agilent CE Capillary Electrophoresis System equipped with an Agilent 6210 Time-of-Flight mass spectrometer, Agilent 1100 isocratic HPLC pump, Agilent G1603A CE-MS adapter kit and Agilent G1607A CE-ESI-MS sprayer kit (Agilent Technologies, Waldbronn, Germany). Detailed methods were as previously described (Ohashi et al., 2008; Qin et al., 2011).

2.5. Data analysis for CE-TOFMS

Raw data obtained by CE-TOFMS were analyzed with KEIO Master Hands software (Sugimoto et al., 2010a). Data analysis was performed using the raw data and included noise filtering, baseline correction, peak detection, deconvolution and integration of the peak area from sliced electropherograms with a 0.02 mass-to-charge ratio (m/z). Detailed methods were as previously described (Sugimoto et al., 2010a). To quantify the major metabolites, the injected volume for CE and the sensitivity of MS were corrected using internal standards, and then all annotated metabolites were further corrected with the same chemicals in a standard mixture to overcome the effect of different ionization patterns.

2.6. Identification of metabolites

Detailed methods are as previously described (Sugimoto et al., 2010b). Briefly, the peaks were identified based on the matched m/z values and normalized migration times of the corresponding standard compounds.

2.7. Immunofluorescence

On DoD12, differentiated cells were immunolabeled with human anti-microtubule-associated protein 2 (MAP2; M4403, 1:200 dilution; Sigma–Aldrich) or anti-tyrosine hydroxylase (TH; AB152, 1:200 dilution; Millipore) antibodies and Hoechst 33342 solution (Dojindo, Tokyo, Japan). Cells were fixed with 4% paraformaldehyde for 15 min and then blocked for 30 min in PBT buffer (phosphate-buffered saline with 5% goat serum and 0.1% Triton). Cells with primary antibodies were incubated overnight at 4 °C. On the next day, cells were washed and blocked in BBT-BSA (bicine-buffered saline with 1 mM $CaCl_2$, 0.1% Triton and 0.5% bovine serum albumin) and then incubated with Alexa-conjugated secondary antibodies (1:1000 dilution; Alexa Fluor 546, Invitrogen).

2.8. Morphological analysis

The immunofluorescence images were acquired using the IN Cell Analyzer 6000 (GE Healthcare, Buckinghamshire, UK) with 6

biological replicates. Each neural cell image was analyzed using image analysis software IN Cell Developer Tool Box 1.7 (GE Healthcare).

2.9. Statistical and multivariate analysis

Statistical significance was assessed using a two-tailed Student's *t*-test and a non-parametric test, the Mann–Whitney *U* test (Qin et al., 2012a,b). Values of $P < 0.05$ were considered to indicate statistical significance. We used unsupervised principal component analysis (PCA) for obtaining a general overview of the variance of metabolites and hierarchical clustering analysis (HCA) for finding relatively homogeneous clusters of cases based on the metabolite profile in SIMCA-P+ (Version 12.0; Umetrics, Umeå, Sweden). A map of the metabolic pathways was obtained from the Kyoto Encyclopedia of Genes and Genomes (KEGG; http://www.genome.jp/kegg/), which is a publicly available web-based tool.

3. Results

3.1. Metabolites of hNPCs identified by CE-TOFMS

A total of 141 peaks (63 positive peaks and 78 negative peaks) were detected by CE-TOFMS analysis, of which 74 principal metabolites (35 cationic species and 39 anionic species) were quantified (Table S1). These metabolites are associated with glycolysis/glyconeogenesis, the pentose phosphate pathway, the tricarboxylic acid cycle, the urea cycle, purine metabolism, pyrimidine metabolism, nicotinate and nicotinamide metabolism, and amino acid metabolism.

3.2. Effect of thalidomide on the metabolism of hNPCs

To identify metabolites associated with thalidomide treatment, PCA and HCA were applied to intercellular metabolic profiles (Fig. 2). A PCA scores plot demonstrated a very clear distinction between intracellular metabolites of cells with and without thalidomide treatment according to the first component (PC1), which represents 95.0% of the total variance. It should be noted that differences in the PCA and HCA were identified using an unsupervised analysis, without any prior information on the samples. Since all cells were cultured under identical conditions, the observed difference demonstrates that the effect of thalidomide treatment is strongly discernible in the individual metabolic profiles. Changes in the major metabolites induced by thalidomide were confirmed by 3 biological replicates. As shown in Fig. 3 and Table 1, we found that levels of tyrosine (Tyr), phenylalanine (Phe), Met and glutathione (GSH), which are involved in dopamine and Met metabolism, were lower in cells treated with thalidomide compared with control cells. However, only GSH was found to be significantly inhibited by thalidomide treatment ($P = 0.049$). A schematic representation of the Tyr and Met metabolic pathways showing the most relevant metabolic changes induced by thalidomide treatment is shown in Fig. 3, based on the KEGG metabolism map.

3.3. Neural differentiation of hNPCs

Expression of a marker of mature neurons (MAP2) and expression of a marker of dopaminergic neurons (TH) were confirmed with an immunofluorescence staining of antibodies on DoD12 (Fig. 4A–C). This suggests that our 12-day hNPC neural differentiation protocol was successful, and that it could be used to assess potential neurological effects of thalidomide (Fig. 4D–F).

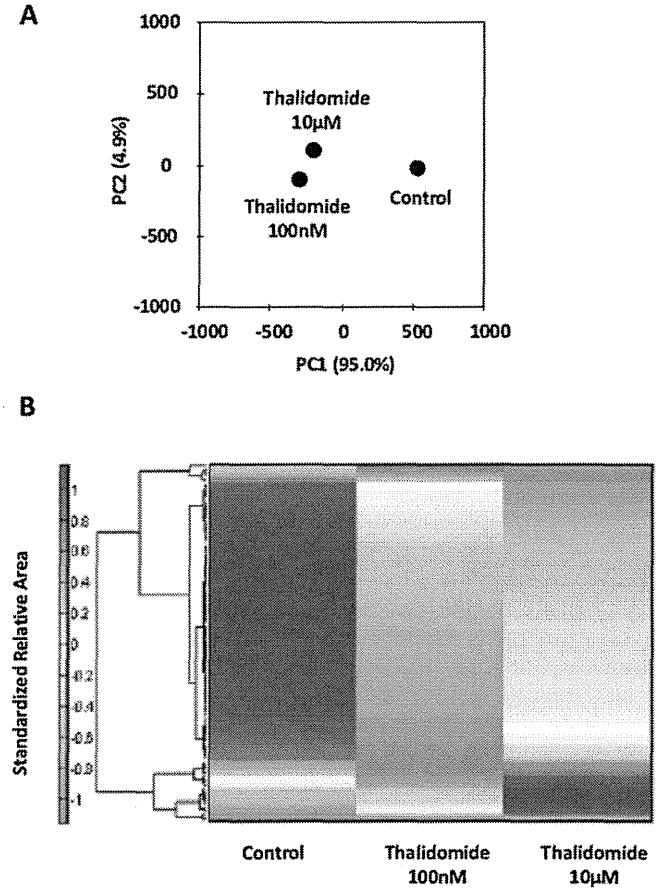

Fig. 2. Metabolomic changes induced by thalidomide during neural differentiation of hNPCs. Cells were treated with DMSO or thalidomide at a concentration of 100 nM or 10 μM during DoD3–5, and metabolite analysis was performed on DoD12 using a CE-TOFMS-based metabolomics technique. PCA score plots (A) and the clusters generated by HCA (B) were applied to the intercellular metabolic profiles to assess thalidomide treatment-related effects. The *Y*- and *X*-axes denote the relative peak area (no units) and the group name, respectively. Each metabolite concentration shown in the heat map was divided by its average, while green and red indicate lower or higher than the average, respectively. (For interpretation of the references to color in this figure legend, the reader is referred to the web version of the article.)

3.4. Effect of thalidomide on dopaminergic neuronal differentiation of hNPCs

Dopamine is a critical neurotransmitter that plays a major role in motor performance, behavior and cognition. The presence of a functional dopaminergic neuron can be considered evidence of the transition from an immature to a mature neuronal progenitor cell. At 100 nM, thalidomide did not produce any significant change in total cell numbers and the length of MAP2-positive neurites. However, 100 nM thalidomide treatments resulted in a significant reduction in the number of TH-positive neurons, compared with control cells (Fig. 4G–I).

4. Discussion

Thalidomide is effective for lepromatous leprosy and multiple myeloma (Sheskin, 1965), and it received US Food and Drug Administration approval for these diseases in 1998 and 2006, respectively (Uhl et al., 2006). However, a major drawback of the use of thalidomide is its diverse neurological side effects. However, little is known of the effects of thalidomide on the pathogenesis of neurodegenerative diseases. Recently, the use of thalidomide has increased. It is generally used at a clinical dose of 100–800 mg per

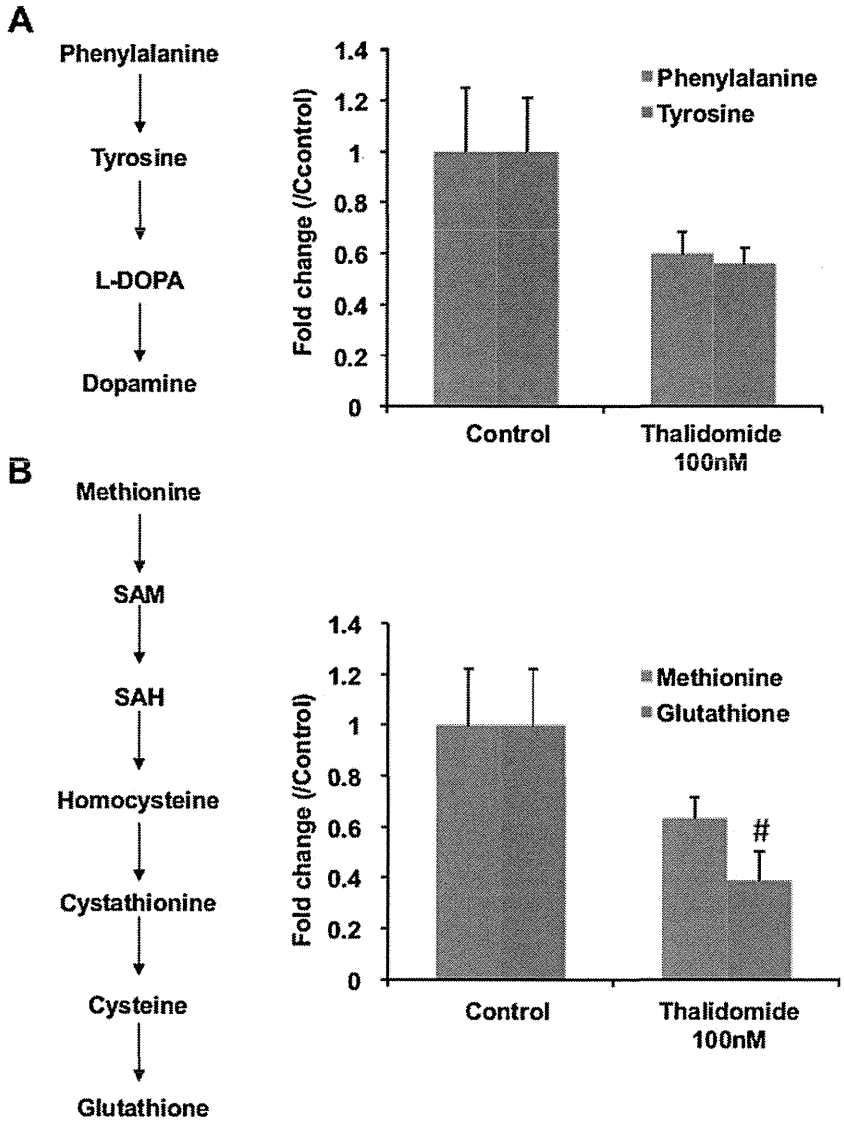

Fig. 3. Effects of thalidomide exposure on Tyr and Met metabolic pathways. Schematic representation of the Tyr (A) and Met (B) metabolic pathways, summarizing the most relevant metabolic changes induced by thalidomide treatment, based on the KEGG metabolism map. Quantitative data are expressed as the mean ± SEM from four independent experiments. $^{\#}P < 0.05$ vs. the vehicle control (0.1% DMSO).

day (Barlogie et al., 2001; Kamikawa et al., 2006). A pharmacokinetic study of low-dose thalidomide in Japanese patients with refractory multiple myeloma found that the plasma concentration of thalidomide 12 h after administration of a dose of 100 mg was 0.85–0.89 μg/ml (approximately 3 μM) (Kamikawa et al., 2006). In the present study, we investigated the effects of thalidomide at 100 nM, which is much lower than its clinical dose, on the metabolism and neuronal differentiation of hNPCs. The cells were exposed to this agent during DoD3–5, and the effects on cellular metabolism and morphology were examined on DoD12.

Table 1
Effect of low dose thalidomide on target metabolites in hNPCs.

Metabolites	Fold change (thalidomide 100 nM vs. DMSO control)		
	Mean	SEM	*P*-Value
Phenylalanine	0.60	0.085	0.18
Tyrosine	0.56	0.064	0.096
Methionine	0.63	0.084	0.17
Glutathione	0.39	0.120	0.049

Values are data from four independent experiments.

In our metabolite analysis, we found that the amounts of Tyr and Phe involved in dopamine metabolism were decreased (but not statistically significant) in thalidomide-treated cells (Fig. 3, Table 1 and Table S1). Furthermore, we found that thalidomide had an inhibitory effect on Met metabolism; we found that the amount of Met was decreased but not significantly in thalidomide-treated cells (Fig. 3, Table 1 and Table S1). Dysregulation of Met metabolism has been implicated in several neurodevelopmental diseases, such as PD and autism (Glaser et al., 2005; James et al., 2004). We also found that 100 nM thalidomide significantly decreased the amount of GSH compared with control cells (Fig. 3, Table 1 and Table S1). GSH is a major antioxidant that protects cells from oxidative stress. Our result is intriguing, as the accumulation of reactive oxygen species (ROS) is considered a risk factor for dopamine cell degeneration in the pathogenesis of PD (Glaser et al., 2005; Wells et al., 2005). Our findings are in agreement with previous studies showing that thalidomide might trigger massive apoptosis in embryonic tissues responsible for limb outgrowth by generating ROS, although oxidative stress was not measured in this present study (Knobloch et al., 2008a,b).

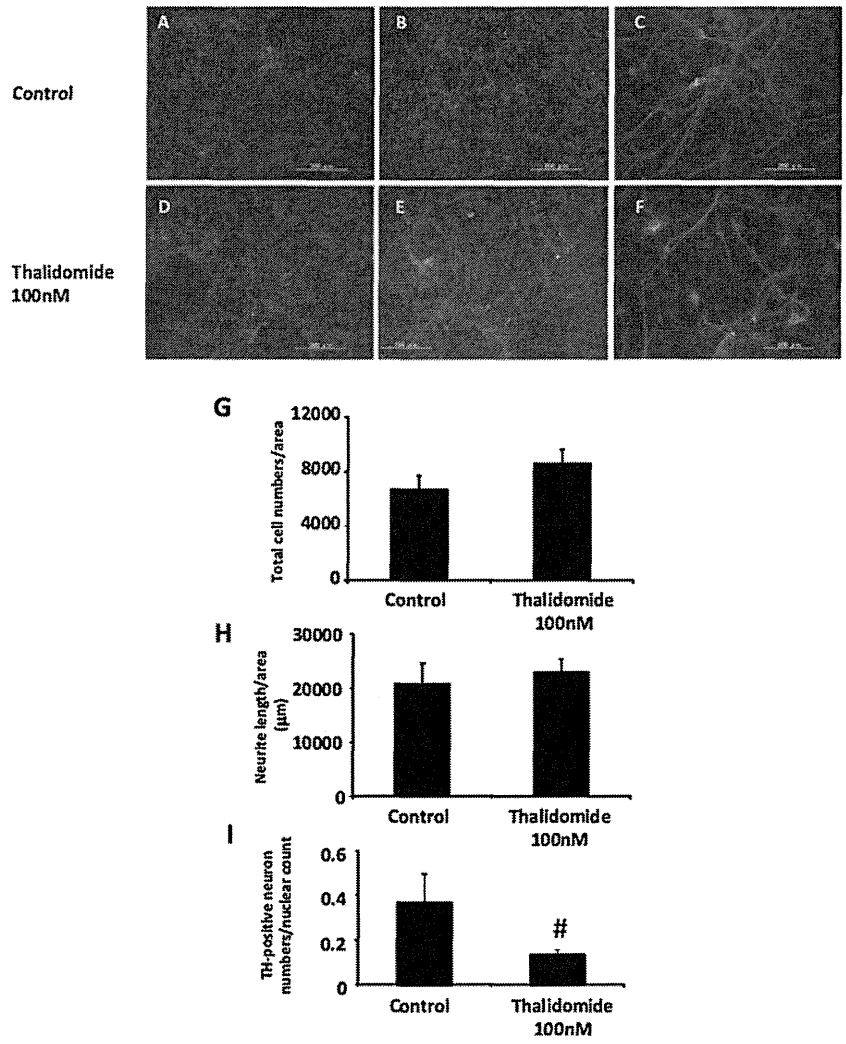

Fig. 4. Thalidomide inhibits dopaminergic neuronal differentiation of hNPCs. Cells were exposed to thalidomide at a concentration of 100 nM during DoD3–5, and morphological analysis was performed on DoD12 using IN Cell Analyzer 6000 with 6 biological replicates. Typical final morphological appearances on DoD12 without (A–C) and with thalidomide treatments (D–F) by the immunocytofluorescence staining. Cells were counterstained with Hoechst (blue) or with MAP2 (red) or TH (green) antibodies. Scale bar is 200 μm. Quantification data of the effects of thalidomide on the number of total cells (G), the relative length of MAP2-positive neurites (H) and the number of TH-positive neurons (I) differentiated from hNPCs. Quantitative data are expressed as the mean ± SEM from six independent experiments. $^{\#}P < 0.05$ vs. the vehicle control (0.1% DMSO).

Another interesting finding of our study is that our morphological analysis indicates that thalidomide treatment at 100 nM significantly decreased the number of TH-positive neurons compared with control cells, although there was no significant effect on MAP2-positive neuronal differentiation (Fig. 4). It has been suggested that low-dose exposure to neurodevelopmental toxins, such as methylmercury, is not associated with gross morphological changes within the developing brain, but rather induces alterations in levels of specific neurotransmitters, such as dopamine (Gimenez-Llort et al., 2001; Zimmer et al., 2011). Our findings appear to support this hypothesis, because the number of TH-positive neurons, but not the number of MAP2-positive neurons, was significantly decreased in thalidomide-treated cells, although dopamine-modulated motor activity was not examined in this study. Dopamine is a monoamine neurotransmitter that plays a critical role in motor performance, behavior and cognition. A progressive loss of dopaminergic neurons is a hallmark of neurodegenerative diseases such as PD (Ebert et al., 2008; Jeon et al., 2010). Transplantation of functional dopaminergic neurons can potentially improve the clinical outcome of PD (Caiazzo et al., 2011; Ma et al., 2011; Sanchez-Pernaute et al., 2008). A possible explanation for our results is that thalidomide decreases the number of dopaminergic (TH-positive) neurons derived from hNPCs. The underlying mechanism might involve the dysregulation of metabolism, release and/or reuptake of dopamine.

In summary, our present study provided possible but limited evidence that thalidomide might inhibit dopaminergic neuronal differentiation of hNPCs at a concentration lower than its clinical dose. The underlying mechanism might involve dysregulation of dopamine and Met metabolic pathways. It should be noted that dopamine neurons are not the only cell type that express TH. Further study is necessary to investigate the effect of low-dose thalidomide on dopaminergic neuronal differentiation in humans. Currently, numerous children are born with thalidomide embryopathy, particularly in Africa and South America, because of the increasing use of thalidomide in treating leprosy (Vianna et al., 2011). Recently, thalidomide was found to have a neuroprotective effect against N-methyl-D-aspartate-induced retinal neurotoxicity, which suggested that thalidomide could potentially be used for the treatment of neurodegenerative diseases (Takada et al., 2011). However, our results suggest that the adverse neurological effects of thalidomide should be taken into

consideration prior to its use in the treatment of neurodegenerative disorders and other diseases.

Conflict of interest statement

The authors declare that they have no financial or non-financial competing interests.

Acknowledgments

We are grateful to Dr. Tin-Tin Win-Shwe for providing us critical comments. This study was supported in part by the Environmental Technology Development Fund (to H.S.) from the Ministry of the Environment and a Grant in Aid for Scientific Research from the Ministry of Health, Labour and Welfare, Japan (to S.O.).

Appendix A. Supplementary data

Supplementary data associated with this article can be found, in the online version, at http://dx.doi.org/10.1016/j.neuro.2012.08.016.

References

Barlogie B, Desikan R, Eddlemon P, Spencer T, Zeldis J, Munshi N, et al. Extended survival in advanced and refractory multiple myeloma after single-agent thalidomide: identification of prognostic factors in a phase 2 study of 169 patients. Blood 2001;98:492–4.

Beal MF, Hyman BT, Koroshetz W. Do defects in mitochondrial energy metabolism underlie the pathology of neurodegenerative diseases? Trends Neurosci 1993;16:125–31.

Breier JM, Gassmann K, Kayser R, Stegeman H, De Groot D, Fritsche E, et al. Neural progenitor cells as models for high-throughput screens of developmental neurotoxicity: state of the science. Neurotoxicol Teratol 2010;32:4–15.

Breier JM, Radio NM, Mundy WR, Shafer TJ. Development of a high-throughput screening assay for chemical effects on proliferation and viability of immortalized human neural progenitor cells. Toxicol Sci 2008;105:119–33.

Caiazzo M, Dell'Anno MT, Dvoretskova E, Lazarevic D, Taverna S, Leo D, et al. Direct generation of functional dopaminergic neurons from mouse and human fibroblasts. Nature 2011;476:224–7.

Ebert AD, Beres AJ, Barber AE, Svendsen CN. Human neural progenitor cells overexpressing IGF-1 protect dopamine neurons and restore function in a rat model of Parkinson's disease. Exp Neurol 2008;209:213–23.

Franks ME, Macpherson GR, Figg WD. Thalidomide. Lancet 2004;363:1802–11.

Gimenez-Llort L, Ahlbom E, Dare E, Vahter M, Ogren S, Ceccatelli S. Prenatal exposure to methylmercury changes dopamine-modulated motor activity during early ontogeny: age and gender-dependent effects. Environ Toxicol Pharmacol 2001;9:61–70.

Glaser CB, Yamin G, Uversky VN, Fink AL. Methionine oxidation, alpha-synuclein and Parkinson's disease. Biochim Biophys Acta 2005;1703:157–69.

James SJ, Cutler P, Melnyk S, Jernigan S, Janak L, Gaylor DW, et al. Metabolic biomarkers of increased oxidative stress and impaired methylation capacity in children with autism. Am J Clin Nutr 2004;80:1611–7.

Jeon SM, Cheon SM, Bae HR, Kim JW, Kim SU. Selective susceptibility of human dopaminergic neural stem cells to dopamine-induced apoptosis. Exp Neurobiol 2010;19:155–64.

Kamikawa R, Ikawa K, Morikawa N, Asaoku H, Iwato K, Sasaki A. The pharmacokinetics of low-dose thalidomide in Japanese patients with refractory multiple myeloma. Biol Pharm Bull 2006;29:2331–4.

Kim JH, Scialli AR. Thalidomide: the tragedy of birth defects and the effective treatment of disease. Toxicol Sci 2011;122:1–6.

Kitiyanant N, Kitiyanant Y, Svendsen CN, Thangnipon W. BDNF-, IGF-1- and GDNF-secreting human neural progenitor cells rescue amyloid beta-induced toxicity in cultured rat septal neurons. Neurochem Res 2011;37:143–52.

Knobloch J, Reimann K, Klotz LO, Ruther U. Thalidomide resistance is based on the capacity of the glutathione-dependent antioxidant defense. Mol Pharm 2008;5:1138–44.

Knobloch J, Schmitz I, Gotz K, Schulze-Osthoff K, Ruther U. Thalidomide induces limb anomalies by PTEN stabilization, Akt suppression, and stimulation of caspase-dependent cell death. Mol Cell Biol 2008;28:529–38.

Lapainis T, Rubakhin SS, Sweedler JV. Capillary electrophoresis with electrospray ionization mass spectrometric detection for single-cell metabolomics. Anal Chem 2009;81:5858–64.

Lenz W. A short history of thalidomide embryopathy. Teratology 1988;38:203–15.

Lunn JS, Sakowski SA, Hur J, Feldman EL. Stem cell technology for neurodegenerative diseases. Ann Neurol 2011;70:353–61.

Ma Y, Peng S, Dhawan V, Eidelberg D. Dopamine cell transplantation in Parkinson's disease: challenge and perspective. Br Med Bull 2011;100:173–89.

Maletic-Savatic M, Vingara LK, Manganas LN, Li Y, Zhang S, Sierra A, et al. Metabolomics of neural progenitor cells: a novel approach to biomarker discovery. Cold Spring Harb Symp Quant Biol 2008;73:389–401.

Matthews SJ, McCoy C. Thalidomide: a review of approved and investigational uses. Clin Ther 2003;25:342–95.

Ohashi Y, Hirayama A, Ishikawa T, Nakamura S, Shimizu K, Ueno Y, et al. Depiction of metabolome changes in histidine-starved *Escherichia coli* by CE-TOFMS. Mol Biosyst 2008;4:135–47.

Qin XY, Fukuda T, Yang L, Zaha H, Akanuma H, Zeng Q, et al. Effects of bisphenol A exposure on the proliferation and senescence of normal human mammary epithelial cells. Cancer Biol Ther 2012;13:296–306.

Qin XY, Kojima Y, Mizuno K, Ueoka K, Muroya K, Miyado M, et al. Identification of novel low-dose bisphenol a targets in human foreskin fibroblast cells derived from hypospadias patients. PLoS One 2012;7:e36711.

Qin XY, Wei F, Yoshinaga J, Yonemoto J, Tanokura M, Sone H. siRNA-mediated knockdown of aryl hydrocarbon receptor nuclear translocator 2 affects hypoxia-inducible factor-1 regulatory signaling and metabolism in human breast cancer cells. FEBS Lett 2011;585:3310–5.

Ryu JK, Cho T, Wang YT, McLarnon JG. Neural progenitor cells attenuate inflammatory reactivity and neuronal loss in an animal model of inflamed AD brain. J Neuroinflamm 2009;6:39.

Sanchez-Pernaute R, Lee H, Patterson M, Reske-Nielsen C, Yoshizaki T, Sonntag KC, et al. Parthenogenetic dopamine neurons from primate embryonic stem cells restore function in experimental Parkinson's disease. Brain 2008;131:2127–39.

Sheskin J. Thalidomide in the treatment of lepra reactions. Clin Pharmacol Ther 1965;6:303–6.

Shin S, Dalton S, Stice SL. Human motor neuron differentiation from human embryonic stem cells. Stem Cells Dev 2005;14:266–9.

Soga T, Ueno Y, Naraoka H, Ohashi Y, Tomita M, Nishioka T. Simultaneous determination of anionic intermediates for *Bacillus subtilis* metabolic pathways by capillary electrophoresis electrospray ionization mass spectrometry. Anal Chem 2002;74:2233–9.

Sugimoto M, Hirayama A, Robert M, Abe S, Soga T, Tomita M. Prediction of metabolite identity from accurate mass, migration time prediction and isotopic pattern information in CE-TOFMS data. Electrophoresis 2010;31:2311–8.

Sugimoto M, Wong DT, Hirayama A, Soga T, Tomita M. Capillary electrophoresis mass spectrometry-based saliva metabolomics identified oral, breast and pancreatic cancer-specific profiles. Metabolomics 2010;6:78–95.

Takada K, Munemasa Y, Kuribayashi J, Fujino H, Kitaoka Y. Protective effect of thalidomide against N-methyl-D-aspartate-induced retinal neurotoxicity. J Neurosci Res 2011;89:1596–604.

Teo SK, Stirling DI, Zeldis JB. Thalidomide as a novel therapeutic agent: new uses for an old product. Drug Discov Today 2005;10:107–14.

Uhl K, Cox E, Rogan R, Zeldis JB, Hixon D, Furlong LA, et al. Thalidomide use in the US: experience with pregnancy testing in the S.T.E.P.S. programme. Drug Saf 2006;29:321–9.

Vianna FS, Lopez-Camelo JS, Leite JC, Sanseverino MT, Dutra Mda G, Castilla EE, et al. Epidemiological surveillance of birth defects compatible with thalidomide embryopathy in Brazil. PLoS One 2011;6:e21735.

Wells PG, Bhuller Y, Chen CS, Jeng W, Kasapinovic S, Kennedy JC, et al. Molecular and biochemical mechanisms in teratogenesis involving reactive oxygen species. Toxicol Appl Pharmacol 2005;207:354–66.

Zimmer B, Schildknecht S, Kuegler PB, Tanavde V, Kadereit S, Leist M. Sensitivity of dopaminergic neuron differentiation from stem cells to chronic low-dose methylmercury exposure. Toxicol Sci 2011;121:357–67.

frontiers in GENETICS

ORIGINAL RESEARCH ARTICLE
published: 07 August 2012
doi: 10.3389/fgene.2012.00141

Identification of stage-specific gene expression signatures in response to retinoic acid during the neural differentiation of mouse embryonic stem cells

Hiromi Akanuma[1], Xian-Yang Qin[1,2], Reiko Nagano[1], Tin-Tin Win-Shwe[3], Satoshi Imanishi[1], Hiroko Zaha[1], Jun Yoshinaga[2], Tomokazu Fukuda[4], Seiichiroh Ohsako[5] and Hideko Sone[1]*

[1] Health Risk Research Section, Center for Environmental Risk Research, National Institute for Environmental Studies, Tsukuba, Ibaraki, Japan
[2] Department of Environmental Studies, Graduate School of Frontier Science, The University of Tokyo, Kashiwa, Chiba, Japan
[3] Biological Impact Research Section, Center for Environmental Health Sciences, National Institute for Environmental Studies, Tsukuba, Ibaraki, Japan
[4] Department of Animal Production Science, Graduate School of Agricultural Science, Tohoku University, Sendai, Miyagi, Japan
[5] Center for Disease Biology and Integrative Medicine, Graduate School of Medicine, The University of Tokyo, Tokyo, Japan

Edited by:
Pierre R. Bushel, National Institute of Environmental Health Sciences, USA

Reviewed by:
Ryou Fukushima, Shionogi & Co., Ltd., Japan
Manikandan Jayapal, King Abdulaziz University, Saudi Arabia

***Correspondence:**
Hideko Sone, Health Risk Research Section, Center for Environmental Risk Research, National Institute for Environmental Studies, 16-2 Onogawa, Tsukuba 305-8506, Japan.
e-mail: hsone@nies.go.jp

We have previously established a protocol for the neural differentiation of mouse embryonic stem cells (mESCs) as an efficient tool to evaluate the neurodevelopmental toxicity of environmental chemicals. Here, we described a multivariate bioinformatic approach to identify the stage-specific gene sets associated with neural differentiation of mESCs. We exposed mESCs (B6G-2 cells) to 10^{-8} or 10^{-7} M of retinoic acid (RA) for 4 days during embryoid body formation and then performed morphological analysis on day of differentiation (DoD) 8 and 36, or genomic microarray analysis on DoD 0, 2, 8, and 36. Three gene sets, namely a literature-based gene set (set 1), an analysis-based gene set (set 2) using self-organizing map and principal component analysis, and an enrichment gene set (set 3), were selected by the combined use of knowledge from literatures and gene information selected from the microarray data. A gene network analysis for each gene set was then performed using Bayesian statistics to identify stage-specific gene expression signatures in response to RA during mESC neural differentiation. Our results showed that RA significantly increased the size of neurosphere, neuronal cells, and glial cells on DoD 36. In addition, the gene network analysis showed that glial fibrillary acidic protein, a neural marker, remarkably up-regulates the other genes in gene set 1 and 3, and *Gbx2*, a neural development marker, significantly up-regulates the other genes in gene set 2 on DoD 36 in the presence of RA. These findings suggest that our protocol for identification of developmental stage-specific gene expression and interaction is a useful method for the screening of environmental chemical toxicity during neurodevelopmental periods.

Keywords: mouse embryonic stem cells, neural differentiation, Bayesian network, retinoic acid, toxicity screening

INTRODUCTION

Humans are exposed to environmental chemicals on a daily basis; however, many effects of these chemicals on human health are unclear. Currently, assessment of developmental toxicity on children's health is a large and rapidly growing research field. Children are not "little adults" and have special vulnerabilities to the toxic effects of environmental chemicals. For example, brain development during embryonic stages is an important period when microstructures are formed and axon guidance and synapse formation are induced by neuronal signaling (Lamoury et al., 2006; Ligon et al., 2006). These processes are regulated by stage-specific gene expression during embryonic development. Therefore, it is necessary to develop a more comprehensive and efficient system to identify the stage-specific gene expression signatures in embryonic development and to evaluate the toxicity of environmental chemicals on neural development.

Toxicity testing using embryonic stem cells (ESCs) has been developed as an efficient approach to assess the effect of environmental chemicals on neurodevelopment (Seiler et al., 2006). We have previously reported a mouse embryonic stem cell (mESC) neural differentiation protocol and showed that it could be used as an efficient tool to evaluate the toxic effects of environmental chemicals on neurodevelopment (Nagano et al., 2012). Furthermore, we have previously developed a method to quantitatively and statistically analyze microarray gene expression data using Bayesian networks with a log-linear functional relationship between genes (Toyoshiba et al., 2004, 2006). We proposed that advanced Bayesian network analysis is a necessary tool to understand the accurate linkage in the possible networks and the mechanism of the action of developmentally neurotoxic compounds.

During mammalian fetal development, the most active form of vitamin A, retinoic acid (RA) can pass through the umbilical cord to the fetus and induce axon formation and neural system development. ESCs express high levels of RA receptor (RAR)α in the undifferentiated stage, while RARβ begins to be expressed after

embryoid body (EB) formation (Shiotsugu et al., 2004; Wilson and Maden, 2005; So et al., 2006). A series of RA concentrations were examined to detect neural cell identity during neuronal differentiation from mESC (Okada et al., 2004; Engberg et al., 2010). They reported that the 10^{-8} M of RA would be an optimum dose to induce cerebral and mesencephalic neurons and the 10^{-7} M of RA had capability to induce motor neurons (Kawasaki et al., 2000; Nishimura et al., 2003; Miyazaki et al., 2005).

Therefore, in the present study, we focused on identification of stage-specific gene expressions and analyzed their relationship network during mESC neurodevelopmental period after RA exposure at 10^{-8} and 10^{-7} M, using an advanced Bayesian network analysis.

MATERIALS AND METHODS

CELL CULTURE AND DIFFERENTIATION

B6G-2 mESCs (RIKEN Cell Bank, Tsukuba, Ibaraki, Japan) were maintained in Dulbecco's modified Eagle's medium (Invitrogen, Carlsbad, CA, USA) supplemented with 15% knockout serum replacement (Invitrogen), 100 μM non-essential amino acids (Invitrogen), 100 μM 2-mercaptoethanol (Invitrogen), and 1000 U/ml leukemia inhibitory factor (LIF; Invitrogen) in gelatinized tissue culture dishes. On the first day of differentiation (DoD 0), cells were transferred in to 24 well plate in media without LIF and allowed to form EBs. The media was changed by every 2 days. RA was added during DoD 2–6 to induce neuronal differentiation. On DoD 8, EBs were transferred to L-ornithine/laminin-coated 24 well plates (BD Bio Coat, BD, Franklin Lakes, NJ, USA) and were cultured with neural medium from DoD 22 to DoD 36 to promote further neural differentiation (**Figure 1A**).

IMMUNOCYTOCHEMISTRY AND MORPHOLOGICAL ANALYSIS

On DoD 8 and DoD 36, EBs, and their derivatives were fixed with 4% PFA in PBS for 15 min and then performed immunostaining with the conventional methods. Cells were incubated with primary antibodies overnight at 4°C at the following dilutions: anti-microtubule-associated protein 2 (*Map2*) antibody (Sigma-Aldrich, Poole, UK; 1:200) and mouse anti-glial fibrillary acidic protein (*Gfap*) monoclonal antibody (Chemicon International,

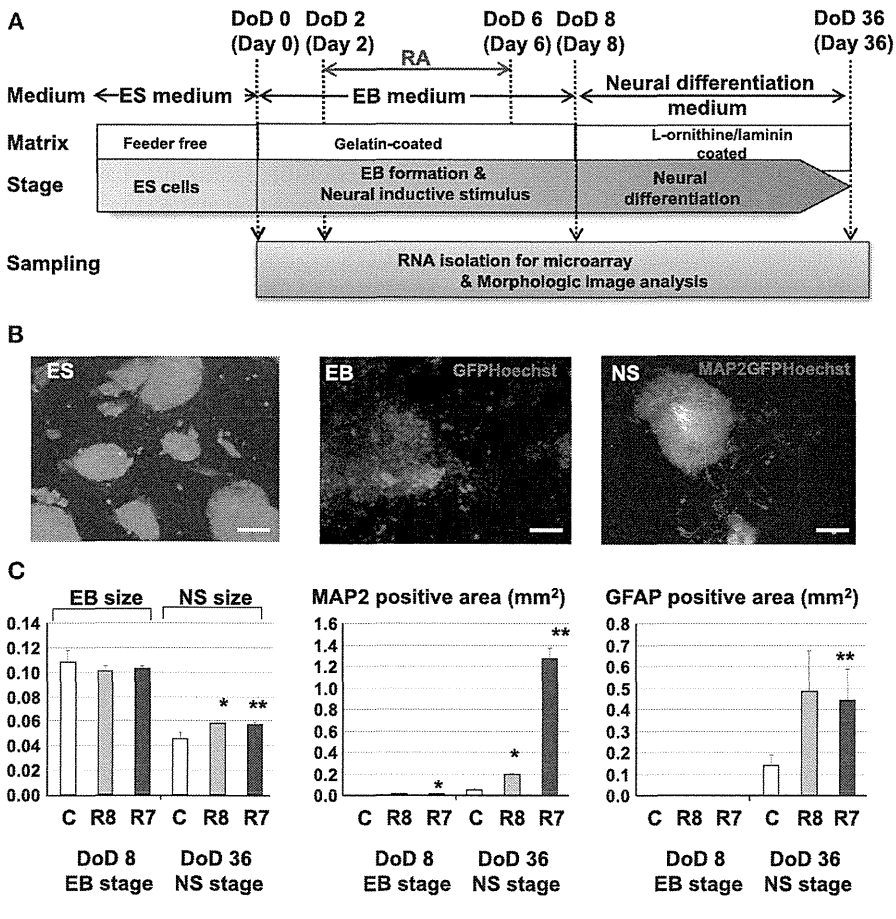

FIGURE 1 | Experimental protocols and morphological analysis of the effect of RA on the neural differentiation of mESCs. (A) A Schematic diagram of cell cultures and chemical exposures. **(B)** Pictures of mESCs, EBs, and neurospheres (NS) with neurite growth derived from neurosphere in fluorescent fields. Green, blue, and red fluorescent images indicate GFP of cytoskeleton proteins, nuclei stained with Hoechst and neuronal cells and neurites stained with the anti *Map2* antibody. Scale bar is 100 μm. **(C)** Morphological analysis of neuronal cell lineages exposed to RAs. Comparison of the EB areas on DoD 8 and DoD 36 showed that the EB area decreased with neuronal cell development. In RA-treated EBs, the numbers of *Map2*-positive axons and *Gfap*-positive cells were increased compared with the control. Symbols of C, R8, and R7 indicate vehicle control, RA 10^{-8} M, and RA 10^{-7} M.

Temecula, CA, USA; 1:200). Cells were rinsed with PBS and then incubated with Alexa-conjugated secondary antibodies (1:1000, Alexa Fluor 546, Invitrogen). Hoechst 33342 solution (Dojindo Laboratories, Kumamoto, Japan) was used for counter-staining. Immunofluorescence images were acquired with six biological replicates per condition using an IN Cell Analyzer 1000 (GE Healthcare, Buckinghamshire, UK) and analyzed using IN Cell Developer Tool Box 1.7 (GE Healthcare). All morphological analysis experiments were performed in triplicate to test the reproducibility of the results. Statistical analysis was performed using two-tailed Student's t-test. Relationships were considered statistically significant with $p < 0.05$.

DNA MICROARRAY ANALYSIS

Total RNA was isolated on DoD 0, 2, 8, and 36 with six biological replicates. And then, single mixed RNA sample per condition was applied to Illumina MouseWG-6v1.0 expression BeadChips covering 46,643 transcripts including 26,766 annotated coding transcripts 2, according to the manufacturer's instructions (Illumina, San Diego, CA, USA). The arrays were scanned in accordance with the manufacturer's directions. Raw expression values of each gene were normalized with median centered by GeneSpring GX10.02 software (Agilent Technologies, Palo Alto, CA, USA). Normalized data were deposited in the National Center for Biotechnology Information Gene Expression Omnibus[1] (accession no. GSE37602).

SELECTION OF GENE SETS

To capture gene expression signatures of stage-specific changes during neural differentiation of mESCs, we performed three approaches to determine gene sets for Bayesian network analysis. Marker genes, which are commonly used to analyze pluripotency and development of neural cells, were selected as the literature-based gene set (set 1) by review of the published literature. The analysis-based gene set (set 2) was selected by the combined use of the knowledge-based database and the following classification methods. Candidate genes involved in axon guidance maps, the nerve growth factor (NGF) pathway, and RA signaling were preliminarily selected from the Kyoto Encyclopedia of Genes and Genomes (KEGG) pathway database[2] and then genes with specific expression patterns were identified using SOM and PCA. Finally, the enrichment gene set (set 3) was selected by clustering expression values of candidate genes contained in the Neurogenesis and Neural Stem Cell PCR Array (SABiosciences, Valencia, CA, USA) using SOM and PCA. SOM and PCA were performed using GeneSpring GX10.02 software (Agilent Technology). Briefly, SOM clustering was done by conditions in which similarity measure: euclidean, maximum number of iterations: 50, numbers of grid rows and columns were 2×4. Then each eight clusters of SOM were analyzed by PCA with four components of eigenvalues (component 1 was more than 40% and component 2 was 10%). To develop set 2 and 3, we collected genes with maximum and minimum values in the PCA component 1 from each SOM cluster.

[1] www.ncbi.nlm.nih.gov/geo

[2] http://www.genome.jp/kegg/pathway.html

GENE INTERACTION NETWORK ANALYSIS

We used a modified gene interaction network (GIN) based on our previous studies (Yamanaka et al., 2004; Toyoshiba et al., 2006; Nagano et al., 2012). The GIN was quantified to calculate the posterior probability distribution for the strength of the linkages based on gene expression and chemical exposure dose datasets. Briefly, a GIN consists of a collection of P nodes, denoted G_1, G_2, ..., G_P, with observed values n_1, n_2, ... n_p. βij ($i, j = 1, 2, \ldots, P$) are parameters in the log-linear function form describing the linkage from node i to node j. Mathematically, this is written as

$$E\left[\log\left(G_j\right)\right] = \sum_{i=1,\neq j}^{P} I_{ij}\beta_{ij}\log\left(n_i\right)$$

where $E[\log(G_j)]$ represents the expectation for the natural logarithm of G_j, and $I_{ij}(i, j = 1, 2, \ldots, P)$ is an indicator function that equals 1 if node G_i has a link to node G_j, otherwise it equals 0. If a node has a regulatory effect on node G_i, then that node is referred to as a "Parent of node G_i," and we refer to it as belonging to the set Pa (G_i). The prior distribution for I_{ij} was assumed to be a Bernoulli distribution with success probability p_{ij} when $Iij = 1$. In the uninformative case, p_{ij} could be set to 0.5 and if there is some expectation that I_{ij} is not equal to zero, the prior probability could be set higher. The posterior distributions for the linkages were derived using Gibbs sampling. The network was used to evaluate the ability of the algorithm to have a higher posterior probability (p-value). Transition matrices were generated at $p > 0.5$.

RESULTS

EFFECTS OF RA ON NEURAL DIFFERENTIATION

Exposure to RA at different concentrations during EB formation induced neuronal and glial cell lineages from mESCs (**Figure 1A**). Morphological analysis with immunofluorescent staining showed that RA significantly increased the size of neurosphere, neuronal cells, and glial cells at DoD 36 (**Figures 1B,C**).

GENE SET SELECTION FOR GENE NETWORK ANALYSIS

To investigate transcriptomic changes as a result of neuronal differentiations and influences of RAs, a cDNA microarray was used to compare expression levels with and without the RA treatments in EB formations and neurosphere developments by hierarchical clustering methods (**Figure 2A**). From 22,188 transcripts presented from eight microarrays, 1,157 transcripts with expression differences greater than 2.0-fold in at least 1 microarray were selected for further analysis. From the microarray analysis, *Nanog* as a marker of undifferentiated ESCs and, *Nestin*, *Map2*, and *Gfap* as markers of neural cells were differentially expressed by RA treatments at differential doses during the neural differentiation of mESCs, suggesting that our protocol could detect the effects of RA on neuronal differentiation (**Figure 2B**). A high level of *Nanog* expression on DoD 8 was decreased in a dose-dependent fashion following RA treatments, but not on DoD 36. *Nestin* expression was increased by the 10^{-7} M RA treatment on DoD 8 and DoD 36. *Map2* and *Gfap* expressions were also increased by RA treatments on DoD 8 and DoD 36 (**Figure 2B**).

Three gene sets were selected for the Bayesian network analysis by our strategies as shown in **Figure 2C**. Selected gene sets are

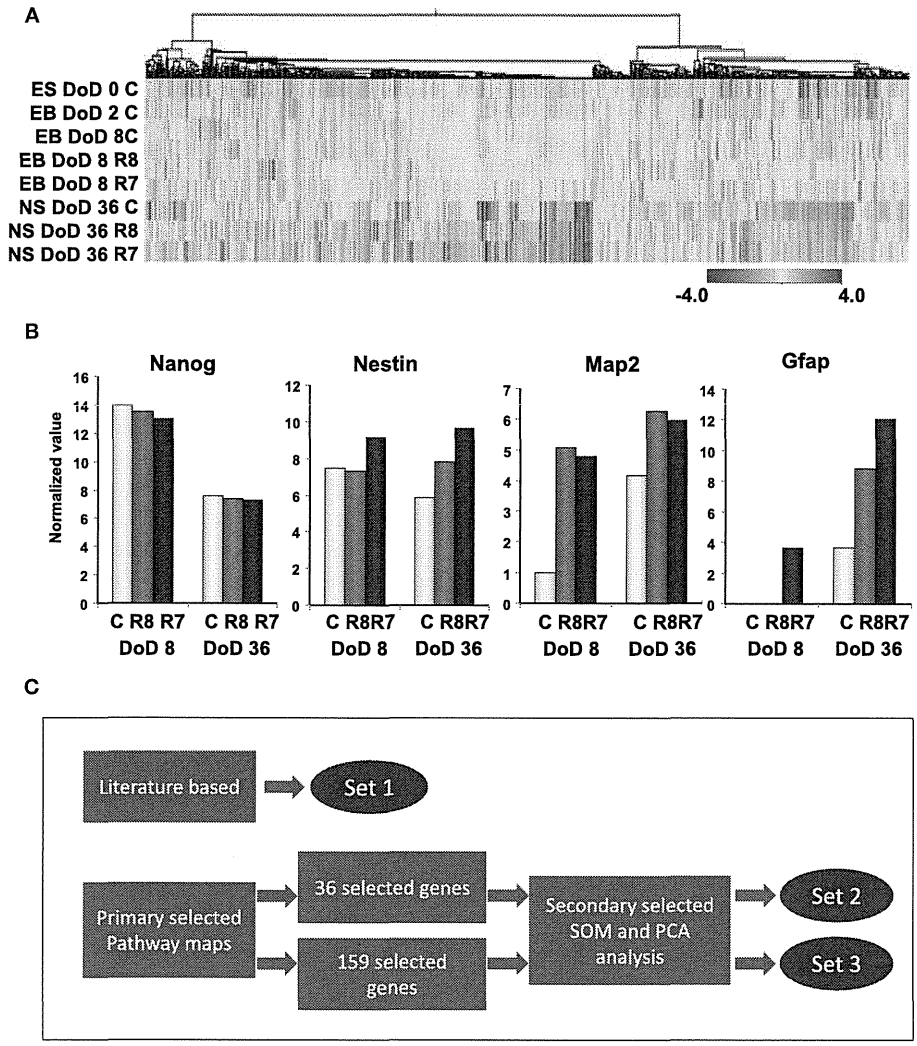

FIGURE 2 | Gene expression analysis by DNA microarray and gene selection strategies for the Bayesian network analysis of differentiation of neuronal cells derived from mESCs. (A) Heat map of hierarchical clustering generated from DNA microarray data. Color-coding in the heat map is that blue from red indicates – 4.0 from 4.0 log2 normalized intensity value by ES values, indicating that red is for up regulation and blue is for down regulation. **(B)** Gene expression of pluripotency and differentiation markers in mESCs, EB, and NS measured in DNA microarray. Symbols of C, R8, and R7 indicate vehicle control, RA 10^{-8} M, and RA 10^{-7} M. **(C)** Stage-specific gene expression signatures in response to RA during the neural differentiation of mESCs were identified as follows: set 1 was a set of genes selected from the literature; set 2 was selected by SOM and PCA after selecting 36 genes from pathway maps; set 3 was selected by SOM and PCA after selecting 159 genes from pathway maps. Expression values of microarray data corresponding to genes in these three sets were used for the Bayesian network analysis.

listed in **Table 1**. Concretely, set 1 was selected by the review of published articles and included *Nanog* (Mitsui et al., 2003; Loh et al., 2006), *Pou5f1* (Okazawa et al., 1991; Catena et al., 2004; Akamatsu et al., 2009), *Zfl42* (Shi et al., 2006; Scotland et al., 2009), *Fgfr1* (Jukkola et al., 2006; Yang et al., 2008; Lee et al., 2009), *Sox2* (Tomioka et al., 2002; Graham et al., 2003; Tanaka et al., 2004; Jin et al., 2009), and *Oligo2* (Ahn et al., 2008). *RARs* were also added to set 1 to assess the effects of RA. Set 2 was selected by the combined use of the KEGG database and SOM and PCA classification methods. Firstly, a list of 36 candidate genes was compiled according to axon guidance, NGF pathway, and RA signaling of KEGG database. It is known that NGF can induce neuronal differentiation of mESCs (Schuldiner et al., 2001) while RA can induce the expression of the NGF receptor (p75) during the neuronal differentiation of PC12 cells (Cosgaya et al., 1996). Therefore, genes in the NGF pathway were selected as indicators to assess the effects of RA on the neural differentiation of mESCs. The 36 candidate genes were then classified in to 17 classes by SOM, and representative genes were selected from each class by PCA. Finally, 16 genes were selected for set 3 by SOM and PCA clustering from 159 candidate genes contained in the Neurogenesis and Neural Stem Cell PCR Array (SABiosciences). Furthermore, specific markers for astrocytes (*Gfap*), mature neurons (*Map2*), neuronal stem cells (*Nestin*), and young neurons (*Tuj1*) were added to sets 2 and 3 to assess the stage of neuronal differentiation.